ISTANBUL TECHNICAL UNIVERSITY ★ INFORMATICS INSTITUTE

INVESTIGATION OF DRUG RESISTANCE MECHANISMS FOR ANTIANDROGEN PROSTATE CANCER DRUG ENZALUTAMIDE USING MOLECULAR DYNAMICS SIMULATIONS

M.Sc. THESIS

Behzad Aslani Avilaq

Department of Applied Informatics

Applied Informatics Programme

Thesis Advisor: Asst. Prof. Sefer BADAY

JULY, 2020

ISTANBUL TECHNICAL UNIVERSITY ★ INFORMATICS INSTITUTE

INVESTIGATION OF DRUG RESISTANCE MECHANISMS FOR ANTIANDROGEN PROSTATE CANCER DRUG ENZALUTAMIDE USING MOLECULAR DYNAMICS SIMULATIONS

M.Sc. THESIS

Behzad Aslani Avilaq
(708171003)

Department of Applied Informatics

Applied Informatics Programme

Thesis Advisor: Asst. Prof. Sefer BADAY

JULY, 2020

İSTANBUL TEKNİK ÜNİVERSİTESİ ★ BİLİŞİM ENSTİTÜSÜ

MOLEKÜLER DINAMİK SIMULASYONLARI KULLANARAK PROSTAT KANSERİNDE KULLANILAN ENZALUTAMİD ILACINA KARŞI GELİŞEN İLAÇ DİRENÇ MEKANİZMASININ ARAŞTIRILMASI

YÜKSEK LİSANS TEZİ

Behzad Aslani Avilaq
(708171003)

Bilişim Uygulamaları Anabilim Dalı

Bilişim Uygulamaları Programı

Tez Danışmanı: Dr.Öğr.Üyesi Sefer BADAY

TEMMUZ, 2020

Behzad Aslani Avilaq, a M.Sc. student of ITU Informatics Institute student ID 708171003, successfully defended the thesis entitled “INVESTIGATION OF DRUG RESISTANCE MECHANISMS FOR ANTIANDROGEN PROSTATE CANCER DRUG ENZALUTAMIDE USING MOLECULAR DYNAMICS SIMULATIONS”, which he prepared after fulfilling the requirements specified in the associated legislations, before the jury whose signatures are below.

Thesis Advisor :	**Asst. Prof. Sefer BADAY** Istanbul Technical University	.....
Jury Members :	**Asst. Prof. Bülent BALTA** Istanbul Technical University	.....
	Asst. Prof. Özge ŞENSOY Medipol University	.....

Date of Submission : 15 June 2020

Date of Defense : 14 July 2020

FOREWORD

Hereby I would like to express my sincere gratitudes to my very supportive advisor, prof. Sefer Baday, from whom I have learned many amazing things in research and in life.

This work has been funded by Career Development Program (3501) of The Scientific and Technological Research Council of Turkey (TUBITAK) (Grant Agreement Number: 117Z353).

Calculations reported in this work were performed at National Center for High Performance Computing of Turkey (UHeM), and at TUBITAK ULAKBIM High Performance and Grid Computing Center (TRUBA resources).

July 2020 Behzad Aslani Avilaq

TABLE OF CONTENTS

Page

FOREWORD ..... **vii**
TABLE OF CONTENTS ..... **ix**
ABBREVIATIONS ..... **xi**
SYMBOLS ..... **xiii**
LIST OF TABLES ..... **xv**
LIST OF FIGURES ..... **xvii**
SUMMARY ..... **xix**
ÖZET ..... **xxi**
1. INTRODUCTION **1**
2. LITERATURE REVIEW **5**
3. MATERIALS AND METHODS **7**
3.1. Crystal Structure Selection 7
3.2. Classical Molecular Dynamic (MD) Simulations 7
3.2.1. AR-APO simulations 8
3.2.2. AR-TES simulations 8
3.2.3. AR-ENZ simulations 8
4. RESULTS OF CLASSICAL MD SIMULATIONS **13**
4.1. Clustering Analysis 13
4.2. Cross Correlation Analysis 14
4.3. Principle Component Analysis (PCA) 15
4.4. Root Mean Square Deviation (RMSD) 16
4.5. Root Mean Square Fluctuation (RMSF) 18
5. ACCELERATED MOLECULAR DYNAMICS (AMD) SIMULATIONS **21**
5.1. Clustering Analysis 22
5.2. PCA 23
5.3. Secondary Structure Analysis 24
5.4. RMSD 24

5.5. Re-run of AMD Simulations 25
6. ANALYSES FOR DYNAMICS OF THE REGION AROUND H11 29
6.1. Bend in H11 29
6.2. Tilt Angle in H3 33
6.3. Correlation Between Agonistic/Antagonistic Activity of Enzalutamide and the Bend/NotBend in H11 34
6.4. Distance Based Analysis 34
6.5. Behavior of H12 According to PCA Analysis 36
6.6. Analysis of Effect of Straightened H11 on Movement of H12 37
6.6.1. Changing NotBend to Bend in a structure with NotBend-H11 state 38
6.6.2. Changing Bend to NotBend in a structure with Bend-H11 state 39
6.6.3. Pulling the loop between H11 and H12 away from H10 and H3 40
6.7. A Network Based on Residue Pair Distance 42
6.8. Feature Selection Analysis 43
6.9. Finding the Pathway 45
7. FREE ENERGY PERTURBATION (FEP) SIMULATIONS 49
7.1. FEP Simulations 49
7.2. Analysis of FEP Results 51
8. DISCUSSION 53
9. CONCLUSION 55
REFERENCES 57
APPENDICES 59
APPENDIX A.1 : Binding Energies 59
CURRICULUM VITAE 61

ABBREVIATIONS

AR : Androgen Receptor

MD : Molecular Dynamics

DBD : DNA Binding Domain

NTD : N-Terminal Domain

LBD : Ligand Binding Domain

LBP : Ligand Binding Pocket

AF2 : Second Activation Function

BF3 : Binding Function 3

TES : Testosterone

DHT : Dihydrotestosterone

ENZ : Enzalutamide

WT : Wild-type

NAMD : Nanoscale Molecular Dynamic

VMD : Visual Molecular Dynamic

PCA : Principle Component Analysis

RMSD : Root Mean Square Deviation

RMSF : Root Mean Square Fluctuation

CMD : Classical Molecular Dynamics

AMD : Accelerated Molecular Dynamics

SYMBOLS

Å	: Angstrom
$_{o}$K	: Degree Kelvin
ps	: Picosecond
fs	: Femtosecond
μs	: Microsecond
χ**1**	: Sidechain Angle of Aminoacids
χ**2**	: Another Sidechain Angle of Aminoacids
E_{dihed}	: Total Dihedral Energy
E_{total}	: Total Potential Energy
V_{dihed}	: Total Dihedral Energy From An MD simulation
V_{total}	: Total Potential Energy From An MD simulation
α_{dihed}	: Dihedral Acceleration Factor
α_{total}	: Potential Acceleration Factor
n_{res}	: Number of Residues
n_{atoms}	: Number of atoms
ΔG	: Binding Energy

LIST OF TABLES

Page

Table 1.1 : Known antiandrogens 3
Table 3.1 : Parameters in simulation runs 7
Table 3.2 : Rigid and flexible docking results 9
Table 7.1 : AR-ENZ systems for FEP simulations 49
Table 7.2 : AR-TES FEP simulation results 50
Table 7.3 : Binding energies obtained from FEP simulations of AR-ENZ simulations .52

LIST OF FIGURES

Page

Figure 1.1 : Androgen Receptor Domains 1
Figure 1.2 : Important sites of AR 2
Figure 1.3 : Helices in AR 2
Figure 3.1 : $\chi 1$ and $\chi 2$ angles in a methionine residue 10
Figure 3.2 : $\chi 1$ and $\chi 2$ angles of the most important residues 10
Figure 4.1 : Clustering of AR-ENZ simulations 13
Figure 4.2 : Clustering of all of MD simulations 14
Figure 4.3 : Cross Correlation Analysis of AR-APO and AR-TES systems 14
Figure 4.1 : Cross Correlation Analysis of AR-agonist and AR-antagonist systems 15
Figure 4.2 : PCA Analysis of AR-ENZ systems 16
Figure 4.3 : PCA Analysis of All of MD simulations 16
Figure 4.4 : RMSD of AR-APO and AR-TES simulations 17
Figure 4.5 : RMSD of AR-ENZ simulations 17
Figure 4.6 : RMSD of AR-APO, AR-TES, and AR-ENZ simulations 18
Figure 4.7 : RMSF of means of AR-APO systems and of AR-TES systems 18
Figure 4.8 : RMSF of AR-APO-1 and AR-TES-1 Systems – 3 μs long simulations 19
Figure 4.9 : RMSF of AR-APO, AR-TES, and AR-ENZ systems 19
Figure 4.10 : Representation of residues 695-720, and 880-895 20
Figure 4.11 : Superimposition of the most dominant cluster of all of simulations 20
Figure 5.1 : Clustering of AR-APO AMD and CMD simulations 22
Figure 5.2 : Clustering of AR-TES AMD and CMD simulations 22
Figure 5.3 : PCA of all of AR-APO simulations 23
Figure 5.4 : PCA of all of AR-TES AMD and CMD simulations 23
Figure 5.5 : Secondary structure analysis of all AR-APO-AMD and AR-TES-AMD 24
Figure 5.6 : RMSD of AR-APO and AR- TES AMD and CMD simulations 25
Figure 5.7 : Distance constant as a successful method in avoiding helicity loss in H1 26
Figure 5.8 : Helicity percentage in three trials for AMD simulations 26
Figure 5.9 : Secondary structure analysis of Re-run AMD simulations. 27
Figure 6.1 : The bend in H11: residues 883-888 29
Figure 6.2 : 882I-886M distance for tracking the bend 29
Figure 6.3 : Bend in AR-APO and AR-TES simulations 30
Figure 6.4 : Bend in AR-ENZ simulations 30
Figure 6.5 : Distance between two alpha carbons of residues 882I, and 886M 31
Figure 6.6 : Distribution of distance between residues 882I, and 886M 32
Figure 6.7 : Superimposition of two states with and without the bend in H11 32
Figure 6.8 : RMSF of all bend and NotBend frames for all MD simulations 33
Figure 6.9 : Distribution of tilting angle of H3 next to a depiction of the helix 34
Figure 6.10 : Distance between residues 882I and 886M in Agonists and Antagonists 34

Figure 6.11 : Movement of H12 away from H3.....35
Figure 6.12 : Movement of loop away from H3 35
Figure 6.13 : Movement of loop away from H10. 35
Figure 6.14 : Movement of H12 away from H3 in AMD simulations.....36
Figure 6.15 : Distribution of distance between H3 and H12 - agonists and antagonists 36
Figure 6.16 : PCA analysis of CMD simulations for H12: Behavior of H12 37
Figure 6.17 : PCA analysis of AMD simulations for H12: Behavior of H12 37
Figure 6.18 : Distance between H10 and the loop - NotBend to Bend.....38
Figure 6.19 : Distance between H3 and the loop - NotBend to Bend.....38
Figure 6.20 : Distance between H3 and H12 - NotBend to Bend 39
Figure 6.21 : Distance between H10 and the loop - Bend to NotBend.....39
Figure 6.22 : Distance between H3 and the loop - Bend to NotBend.....40
Figure 6.23 : Distance between H3 and H12 - Bend to NotBend 40
Figure 6.24 : Distance between H10 and the loop - Loop away from H3 and H12.....41
Figure 6.25 : Distance between H3 and the loop - Loop away from H3 and H12 41
Figure 6.26 : Distance between H3 and H12 - Loop away from H3 and H12.....41
Figure 6.27 : Residue networks based on their alpha carbon distance.....42
Figure 6.28 : Important residues interacting with ENZ 43
Figure 6.29 : Interaction of residues LEU880, LEU701, and ASN705 44
Figure 6.30 : Pathway of Bend to NotBend 45
Figure 6.31 : Interaction network based on Interactions analysis from Pycontact 45
Figure 6.32 : Map of intramolecular interactions in all of CMD simulations.....46
Figure 6.33 : Interactions among segments H3, H11, and loop in CMD simulations 46
Figure 6.34 : H-bond interactions between H10, H11, the loop, and H12 in CMDs.....47
Figure 6.35 : Hbond analysis in AMD simulations separated by Bend and NotBend....47
Figure 6.36 : Hbond analysis in AMD simulations - agonist and antagonist 48
Figure 6.37 : Interactions between residues 891 and N705 in AMD simulations 48
Figure 7.1 : Distribution of binding Energies extracted from FEP simulation results....52
Figure 8.1 : Pathway of interactions upon ENZ binding, and movement of H12.....53

INVESTIGATION OF DRUG RESISTANCE MECHANISMS FOR ANTIANDROGEN PROSTATE CANCER DRUG ENZALUTAMIDE USING MOLECULAR DYNAMICS SIMULATIONS

SUMMARY

Prostate cancer is the most common cancer type in males after lung-cancer. It is a leading death reason amongst cancer-related deaths. Several drug molecules have been developed for the treatment of prostate cancer. Among those, Enzalutamide molecule is the most recent and potent one. In clinical studies, Enzalutamide therapy reduced significantly radiographic progression and delayed the need for chemotherapy. Despite this success, recently it has been discovered that drug resistance against Enzalutamide occurred. Development and progression of the prostate cancer depends on the androgen stimulation. Therefore, antiandrogen drug molecules target and inhibit Androgen Receptor (AR) signaling function.

Enzalutamide properly inhibits AR signaling in wild-type ARs, however two point mutations as F876I, and F876L abolish the antagonistic activity of enzalutamide. The molecular mechanisms of this resistance remain elusive. Thus, this study investigated the mechanism of this resistance at the molecular level using Molecular Dynamics (MD) simulations. We performed one micro-second long classical and accelerated MD simulations of WT-AR, AR with Testosterone and, several AR mutants in complex with Enzalutamide. The experimental structure of AR-Enzalutamide complex has not been solved yet. Thus, prior to MD simulation we performed docking of Enzalutamide into androgen receptor.

Current studies suggest that displacement or instability of the H12 might be causing the switch between antagonist to agonist activity. However, what interactions lead to the instability of helix12 have not been understood clearly. Our simulations suggest that unbending of H11 (at the crystal structure it is in bend structure) could lead to the loss in stability of H12. In the simulations of Apo AR and AR with Testosterone, the unbending is rare. On the contrary, the simulations of AR with enzalutamide, particularly with mutations abolishing antagonist activity, the unbending of H11 becomes too frequent. The current study found an important pathway of interactions which lead to drug resistance upon enzalutamide binding.

MOLEKÜLER DINAMİK SIMULASYONLARI KULLANARAK PROSTAT KANSERİNDE KULLANILAN ENZALUTAMİD ILACINA KARŞI GELİŞEN İLAÇ DİRENÇ MEKANİZMASININ ARAŞTIRILMASI

ÖZET

Prostat kanseri, akciğer kanserinden sonra erkeklerde en sık görülen kanser türü olup, kansere bağlı ölümler arasında önde gelen bir ölüm sebebidir. Androjen reseptör (AR) prostat gelişimi ve büyümesinde transkripsiyon faktörü olarak işlev görür ve düzenleyici rol oynar. Aşırı aktif androjen reseptörünün, prostat kanseri hastalığı olan hastalarda aşırı hücre büyümesine veya kanser hücrelerinin çoğalmasına neden olduğu görünmüştür. Doğal androjenik testosteron (TES) ve dihidrotestosteron (DHT) gibi hormonlar androjen reseptörüne bağlanarak ve onu aktif ederek prostat kanseri gelişiminde önemli bir rol oynamaktadır.

Daha önceki çalışmalarda birkaç ilaç molekülü prostat kanseri tedavisi için geliştirilmiştir. Flutamid, Bicalutamid ve Enzalutamid (ENZ) molekülleri, AR-LBP'ye bağlanarak androjenlerin AR'ne bağlanmasını önler. TES ve DHT gibi agonistler AR'nü, AF2 bölgesini stabilize ederek aktif ederler, ancak antagonist bağlanan AF2 bölgesi dengesizleştiğinde AR'nün deaktivasyonuna yol açar.

Yukarıda bahsedilmiş olan antiandrojenler arasında, Enzalutamid molekülü en yeni ve güçlü olanıdır. Klinik çalışmalarda, Enzalutamid tedavisinin radyografik ilerlemeyi önemli ölçüde azalttığı ve kemoterapi ihtiyacını geciktirdiği görülmüştür. Son zamanlardaki çalışmalarda ise Enzalutamid'e karşı ilaç direncinin meydana geldiği tespit edilmiştir.

Prostat kanserinin gelişimi ve ilerlemesi androjen stimülasyonuna bağlıdır. Bu nedenle, antiandrojen ilaç mollekülleri AR sinyal fonksiyonunu hedefler ve inhibe eder. Enzalutamid, doğal-tip ARlerinde AR sinyallemesini düzgün bir şekilde inhibe eder, ancak F876I ve F876L gibi mutasyonlar Enzalutamid'in antagonistik aktivitesini ortadan kaldırır. Bu direncin moleküler mekanizmaları bilinmediğinden, bu çalışmada Moleküler Dinamik simülasyonları kullanılarak bu mekanizmanın moleküler düzeyde araştırılması amaçlanmıştır.

Bu kapsamda WT-AR, AR ile Testosteron ve farklı AR mutantları ile Enzalutamid kompleksinin çeşitli varyasyonlarının yer aldığı 1 mikrosaniye uzunluğunda klasik ve hızlandırılmış MD (AMD) simülasyonları gerçekleştirilmiştir.

AMD simülasyonları ile uzun vadede AR'deki büyük yapısal değişikliklerin yakalanabileceği düşünülmüştür. AR-Enzalutamide kompleksinin deneysel yapısı henüz çözülemediğinden, MD simülasyonundan önce Enzalutamid molekülünün androjen reseptörüne yapı bazlı hesaplamalar ile yerleştirilmesi işlemi yapılmıştır. Belirtilen proteinin davranışı hakkında daha ayrıntılı bilgiye erişebilmek ve ayrıca her bir

simülasyon sisteminin replikasyonu arasındaki kritik farklılıkları belirlemek için her bir sistemin çoklu replikasyonu simüle edilmiştir.

Tüm moleküler dinamik simülasyonları Charmm-gui web sunucusunda Charmm-36 kuvvet alanı parametreleri kullanılarak oluşturulmuştur. Simülasyon sistemlerine TIP3P'ye ait su molekülleri ilave edilmiş ve proteinden 12Å uzaklığa sahip çözünen atomlar ile dikdörtgen şeklinde bir su kutusu oluşturulmuştur. Simülasyonları çalıştırmak için Nano Ölçek Moleküler Dinamik (NAMD) paketi kullanılmıştır.

AR'nün yabani AR (AR-WT) yapısının yanı sıra mutant AR yapıları olan F876I, F876L, F876Y, T877A-F876L ve T877A da kullanılmıştır. Enzalutamid, AR-WT, AR-F876Y ve AR-T877A sistemlerinde antagonist görevi görmekteyken; AR-F876I, AR-F876L, AR-T877A-F876L sistemlerinde agonist görevi görmektedir.

Mevcut çalışmalar, H12'nin yer değiştirmesi veya kararsızlığının, Enzalutamid'in antagonist ile agonist aktiveteleri arasındaki farklılaşmaya neden olabileceğini göstermektedir. Ancak sarmal12'nin kararsızlığına yol açan etkileşimler açıkça anlaşılamamıştır. Bu çalışmada MD ve AMD simülasyonları yapıldıktan sonra, H12'nin hareketine yol açan etkileşimlerle ilgili detaylı bilgi edinebilmek için farklı analizler yapılmıştır.

Bu analizler çoğunlukla Ambertools16, Pycontact ve VMD içindeki bir MD simülasyon analiz aracı olan Cpptraj kullanılarak yapılmış ve Python 2.7 programlama dili ile görselleştirilmiştir.Kümeleme, PCA, RMSD, RMSF, Çapraz Korelasyon etkileşimi ve uzaklık analizleri tüm simülasyonlar için gerçekleştirilmiştir. Simülasyon bazında ihtiyaçlara bağlı olarak sonuçların yorumlanması için simülasyon yörüngeleri üzerinde daha farklı analizler de gerçekleştirilmiştir.

Simülasyon sonuçları, kristal yapıda bükülmüş durumda bulunan H11'deki bükülmenin H12 stabilitesinde kayba yol açabileceğini düşündürmektedir. Apo AR ve AR'nün, Testosteron ile birlikte bulunduğu komplekslerin simülasyonlarında bükülme nadir olarak gözlenmiştir. Aksine, AR'nün Enzalutamid içeren komplekslerin, özellikle antagonist aktiviteyi ortadan kaldıran mutasyonlarla oluşturulan simülasyonlarda, H11 bükülmesinin çok sık gözlendiği görülmüştür.

Ayrıca simülasyon analizlerine göre Enzalutamid bağlanmasının, H11'in direncini kaybetmesini tetiklediği ve H10 ile birlikte düz bir sarmal haline gelmesine neden olduğu çıkarımı yapılmıştır. H11'deki bükülmenin kaybedilmesi ile birlikte, H3 ile H11 ve H12 arasında yer alan döngü arasındaki etkileşimlerin kaybı ile sonuçlandığı görülmüştür. Sonuç olarak bu durum H10 ve H11 arasında daha fazla etkileşime neden olmuş ve bu da onun düz bir sarmal gelmesine neden olmuştur.

MD ve AMD simülasyonlarının sonuçları, antagonist bağlanmanın H12 üzerindeki etkiye yol açan etkileşimlerin agonist bağlanmadakinden farklı olduğunu göstermektedir. ENZ, AR-LBP'ye bağlandığında, Enzalutamid ile L701 ve N705 tortuları arasındaki etkileşimler nedeniyle H11 ve H12 arasında yer alan L701, N705 ve F891 tortuları arasındaki etkileşimler azalmıştır. Bu durumun H3 ile H11 ve H12 arasında yer alan uzaklığın artmasına neden olduğu görülmüştür. Belirtilen döngüdeki esnekliğinin artması nedeniyle H12'nin H3'ten uzaklaşmış olduğu, böylece LBP'den dışarı doğru hareket ettiği gözlenmiştir.

H12'nin hareketi AR'nin AF2 bölgesini bozarak koaktivatör bağlanması için uygun olmayan bir bölge haline gelmesine, sonuç olarak da AR'nin normal transkripsiyon aktivitesinin baskılandığı görülmüştür.

FEP simülasyonlarının sonuçlarında ise ENZ'nin antagonist AR'ye bağlanma enerjisinin, agonist AR'ye bağlanma enerjisinden yüksek olduğu görülmüştür. Bu durumda antagonist ENZ'nin AR'ye daha iyi bağlandığı çıkarımı yapılabilir. Agonist ENZ'nin daha zaif bağlandığı görünmektedir. Bu durumda ENZ AR'nin bağlanma bölgesine bağlanınca gereken etkileşimler sağlanmamaktadır, ve bu nedenle H12'nin bahsedildiği bağlanma bölgesinden uzağa doğru hareketi görünmemektedir. H12 LBP'ten uzaklaşmadığı durumda, AF2 bölgesi bozulmamaktadır. Mevcut çalışma sonucunda Enzalutamid bağlanması üzerine ilaç direncine yol açan önemli etkileşimlerin nasıl oluştuğuna dair detaylı bilgiler elde edilmiştir. Bu etkileşimler yeni ilaç tasarımı için çok önemlidir.

1. INTRODUCTION

Prostate cancer is the most common cancer in men after lung cancer, and it is in the lead for men in the ages between 65 to 74. [1]. It is a leading death reason amongst cancer-related deaths. Prostate cancer progress is shown to depend upon transcriptional activity of androgen receptor. Androgen receptor functions as a transcription factor and regulates development and growth of prostate. Overactive androgen receptor in fact, causes excessive cell growth or duplication of cancer cells in patients with prostate cancer disease.

Androgen receptor consists of three main segments known as the DNA Binding Domain (DBD), the N-Terminal Domain (NTD), and the Ligand Binding Domain (LBD) (Figure 1.1). The LBD of androgen receptor (residues 670 to 919) is the focus of this study, thus it will be referred as AR, for simplicity.

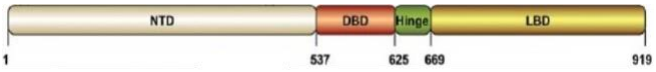

Figure 1.1 : Androgen Receptor Domains.

The most important sites of AR are comprised of a ligand binding pocket (LBP), a second activation function site (AF2), and a Binding Function 3 (BF3). The LBP is in fact for ligands to bind into it and activate or deactivate the AR. AF2 site of AR which is the region covered by helix 3 (H3), H4, H5, and H12, mediates the ligand-dependent transactivation and coactivator recruiting. BF3 on the other hand, is a potential target for engineered peptides or small molecules to bind and change the conformation of AR for many different aims (Figure 1.2). A depiction of helices in AR is shown in Figure 1.3.

Natural androgenic hormones such as testosterone (TES), and dihydrotestosterone (DHT) bind into AR and activate it; thus playing an important role in development of prostate cancer.

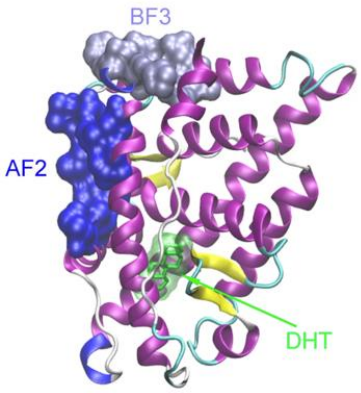

Figure 1.2 : Important sites of AR.

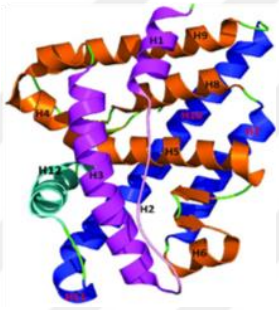

Figure 1.3 : Helices in AR.

So far there are two ways to stop progress of prostate cancer. The first way is to stop the production of androgenic hormones in the body, which is achieved either by surgery or chemical castration. The second way on the other hand, is to suppress normal activity of AR by preventing androgens from binding into it. Antiandrogens such as Flutamide, Bicalutamide, and Enzalutamide (ENZ), bind into AR-LBP and prevent androgens from binding into AR. Agonists such as TES, and DHT activate the AR by stabilizing AF2 site of it, however, upon antagonist binding AF2 site is destabilized, leading to deactivation of AR. Mutations acquired by AR lead to drug resistance, meanwhile leading to agonistic activity of the mentioned antiandrogens. A simple introduction to these antiandrogens is shown as in Table 1.1.

As an antiandrogen drug, ENZ is efficient in overcoming AR mutations which lead to drug resistance against Flutamide, and Bicalutamide. However, new mutations acquired by AR, led to drug resistance against ENZ. The current study aimed to investigate this resistance and factors leading to it.

Table 1.1 : Known Antiandrogens.

Antiandrogen	**FDA approved (year)**	**Agonistic Mutation(s)**	**Structure**
Flutamide	1989	AR-T877A	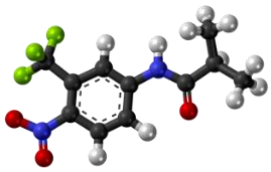
Bicalutamide	1995	AR-W741C	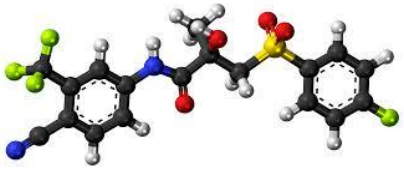
Enzalutamide	2012	AR-F876I AR-F876L AR-T877A-F876L	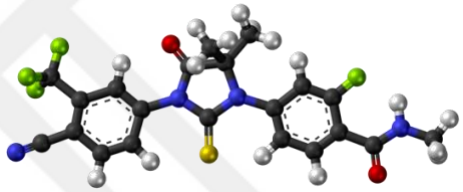

2. LITERATURE REVIEW

Anti-androgens are efficient in treatment of prostate cancer; however inevitable drug resistances occur due to mutations in AR. Introduction of ENZ as an antiandrogen was a success in overcoming mutations acquired by AR against Flutamide and Bicalutamide. However, new mutations in AR, as shown in Table 1.1, transformed ENZ from being an AR-antagonist to an AR-agonist. Korpal and colleagues discovered that the F876I mutation in AR confers genetic and phenotypic resistance to ENZ. [2]. Balbas et al. also introduced the F876L mutation of AR as a resistant factor against ENZ and they proposed a method for overcoming mutation-based resistance to antiandrogens with rational drug design [3]. Many approaches have been discussed in order to overcome these drug resistances [4]. Meanwhile, additional research is needed to investigate mechanism of action of ENZ in order to understand how it works and avoid the drug resistance.

Bassetto et al. did a series of molecular modelling studies that were performed on the AR antagonist conformation, providing useful insights on potential protein-ligand interactions [5].

Interactions between AR and its coactivator is shown to be different upon ligand binding. Moreover, antagonists binding creates stronger interactions between AF2 region and AR's coactivator compared with Apo form of AR. Agonist binding however, leads to weaker interactions between AF2 and the coactivator [6].

As mentioned earlier, the destabilization of AF2 site (H3, H4 and H12) is shown to be due to changes in conformation of AR upon antagonist and or agonist binding. Moreover, the most important factor is change in conformation of H12, which moves away from the LBP, when an antagonist binds into AR. Duan et. al conducted a research in which they performed 1μs-long molecular dynamics simulations in order to find a pathway of interactions leading to conformation change in H12 upon ENZ binding [7]. The loop between H11 and H12 appeared to be very important regarding this change in H12.

Similar studies have been done in order to investigate mechanism of action of ENZ upon binding into AR [8,9]. Utilizing MD simulations, interaction pathways from ENZ to H12 have been introduced upon ENZ binding [10,11]. However, there is no single common and reliable allosteric pathway of interaction upon ENZ binding according to mentioned studies. In order to address this gap in research many simulations with different conformations of AR with ENZ in its LBP, and replications of those systems must be considered. Long-range simulations must be run in order capture the more important changes in conformation of systems. The current study aimed to accomplish this matter and the following section is the methods that we utilized to address it.

3. MATERIALS AND METHODS

3.1. Crystal Structure Selection

A comprehensive search had been conducted in order to find available crystal structures of AR in the PDB Bank, and among those, structure with the PDB id of 2AM9 was chosen due to owning a good resolution (1.64 Å), and no missing residues. There is no crystal structure of a wild-type AR without any ligand bound into its LBP in the literature. Since 2AM9 is the structure of AR with testosterone (TES) bound into it, TES was eliminated from the structure, in order to get the structure of AR itself.

3.2. Classical Molecular Dynamic (MD) Simulations

Multiple replicas of each system were considered in order to acquire a broad understanding of behavior of the protein and also, specify critical differences among replications of every single simulation system. All molecular dynamic simulations were built by utilizing Charmm-gui web server [12], and Charmm-36 force field parameters were used. Water molecules of TIP3P were added to simulation systems, and a rectangular water box was considered with solute atoms with 12Å distance away from the edges of protein. Nanoscale Molecular Dynamic (NAMD)[13] package was used to run the simulations, and the following parameters were considered in simulation runs. (Table 3.1).

Table 3.1 : Parameters in simulation runs.

Parameter	Description
Minimization	10,000 steps
System atom size	60,000
Temperature	303 ºK
Timestep	2 fs
Restart frequency	1 ps
Cutoff	12 Å
Pairlistdist	16 Å

Besides, collective variables also were applied in order to keep the protein inside the solution box.

3.2.1. AR-APO simulations

In order to analyze and observe the behavior of androgen receptor without any ligand in its ligand binding pocket, a system of AR-APO was prepared. Four replicas of the simulation system were launched, and as a matter of curiosity, a fifth replica was also run in which an engineered peptide was present next to the AF2 site. The mentioned peptide (FxxFF) acts as a coactivator and binds to the AF2 site of AR, and is present in the structure with PDB id of 1T73. Besides, the first replication of AR-APO system was extended for a 3 μs-long simulation to address the changes in protein's conformation in long run.

3.2.2. AR-TES simulations

The same procedure as in AR-APO systems, were done in order to prepare AR-TES systems. Structure of AR-TES with PDB id of 2AM9, was used to prepare the systems, and four replica simulations were run. As well as AR-APO, in the case of AR-TES, the first simulation was extended for a 3 μs-long run.

3.2.3. AR-ENZ simulations

3.2.3.1. Docking and structure preparation

The structure with PDB id of 2AM9 was considered as the wild-type (WT) AR structure for docking. Mutations F876I, F876L, F876Y, T877A, and T877A-F876L were applied to the WT-AR structure using Charmm-gui web server, in order to make mutants of AR prior to docking. After 1μs-long AR-APO replica simulations were finished, trajectories of these five simulations were combined and a clustering analysis was employed. The first five structures of clustering analysis results were chosen as five common structures for docking. Besides, another clustering was done for AR-APO1 (an md simulation of 3 μs long) and the first cluster of it (named as APO1), was chosen for further docking. For all chosen structures rigid and flexible dockings were prepared using AutoDockTools [14], and were performed via AutoDock Vina. In order to choose flexible residues in flexible

dockings, residues with either big side chain, or in general those that block a big volume of LBP were chosen. These residues were LEU704, TRP741, MET745, and PHE764. All of AR-ENZ systems are shown in Table 3.2. Note that in flexible dockings the ligand binding score is better (lower binding energy).

Table 3.2 : Rigid and flexible docking results (kcal/mol).

Structure	Docking Type	score	Structure	Docking Type	score	Structure	Docking Type	score
2AM9	Rigid	10.1	2AM9_T877A	Flexible	-7.7	5APOs-c2	Rigid	24.0
2AM9	Flexible	-7.5	2AM9_T877A-F876L	Rigid	2.2	5APOs-c2	Flexible	-6.8
2AM9	Flexible; No741	3.2	2AM9_T877A-F876L	Flexible	-7.7	5APOs-c3	Rigid	3.1
2AM9	Flexible; No741	3.2	2AXA-Balbas	Rigid	1.1	5APOs-c3	Flexible	-7.9
2AM9_F876I	Rigid	-3.3	2AXA-Balbas	Flexible	-7.3	5APOs-c4	Rigid	6.9
2AM9_F876I	Flexible	-6.1	APO1	Rigid	15.1	5APOs-c4	Flexible	-7.0
2AM9_F876L	Rigid	2.7	APO1	Flexible	-6.1			
2AM9_F876L	Flexible	-8.0	5APOs-c0	Rigid	12.1			
2AM9_F876Y	Rigid	10.6	5APOs-c0	Flexible	-6.7			
2AM9_F876Y	Flexible	-8.1	5APOs-c1	Rigid	17.9			
2AM9_T877A	Rigid	6.0	5APOs-c1	Flexible	-3.6			

3.2.3.2. Rotation angles of chosen residues: validation of flexible docking results

In flexible docking, important residues in the LBP were chosen to have flexible sidechains while docking. Critical residues in the ligand binding pocket play an important role in intramolecular and ligand-molecular interactions. Therefore, sidechain angles taken by these residues are important, since they can lead to big changes in ligand binding and conformation changes of the protein. Figure 3.1, is a depiction of sidechain angles (χ_1 and χ_2) of a methionine amino acid. In order to validate the angles that these residues took in flexible dockings a comparison of values of these residues were conducted. This analysis

demonstrates χ_1 and χ_2 angles of the most important residues in the ligand binding pocket of AR in docked systems, AR-APO simulations, and crystal structures (Figure 3.2). As a conclusion, angles of the mentioned residues in flexible dockings were mostly seen in simulations or in crystal structures.

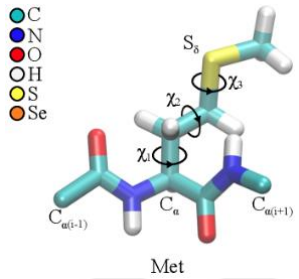

Figure 3.1 : χ1 and χ2 angles in a methionine residue.

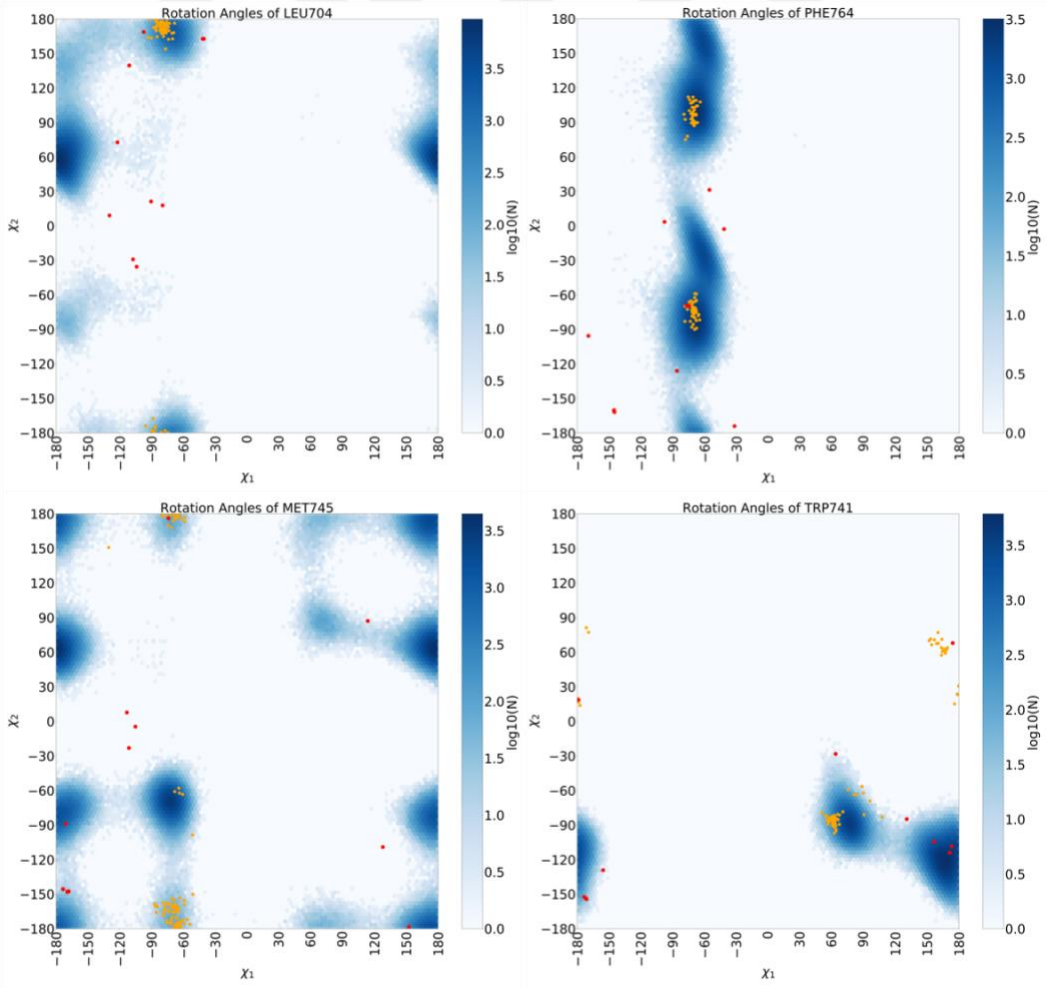

Figure 3.2 : χ1 and χ2 angles of the most important residues in the ligand binding pocket of AR. Dots in red show rotation angles taken by residues in the flexible dockings. Dots in orange show the angles of residues in crystal structures in literature. The light blue color in the background shows the angles acquired by these residues along AR-APO, and AR-TES simulations.

For all of rigidly and flexibly docked systems, simulation systems were run. However, in some of rigidly docked systems after dozens of nanoseconds, due to instability of systems, the ligand was pushed out of the protein. Thus, only flexible docking systems were considered for longer runs and for further analyses.

4. RESULTS OF CLASSICAL MD SIMULATIONS

Analysis of results were mostly done using Cpptraj, a MD simulation analysis tool within Ambertools16 [15], Pycontact [16], and Visual Molecular Dynamic (VMD) [17], and were visualized via Python 2.7 programming language. For all of simulations including the first AR-APO and the first AR-TES that were run for 3 μs, in this step of analysis only the first 1 μs of them were considered.

4.1. Clustering Analysis

Clustering analysis is a way of grouping all frames of simulations into certain number of groups based on their similarity to a reference structure. In this study, we defined the starting point structure of the protein in every simulation as its reference structure. In order to do the clustering analysis, all of simulations were included. As it is demonstrated in Figure 4.1, there are some common clusters for AR-ENZ agonist and or antagonist simulations. AR-ENZ simulations also, have common clusters with AR-APO and AR-TES simulations (Figure 4.2).

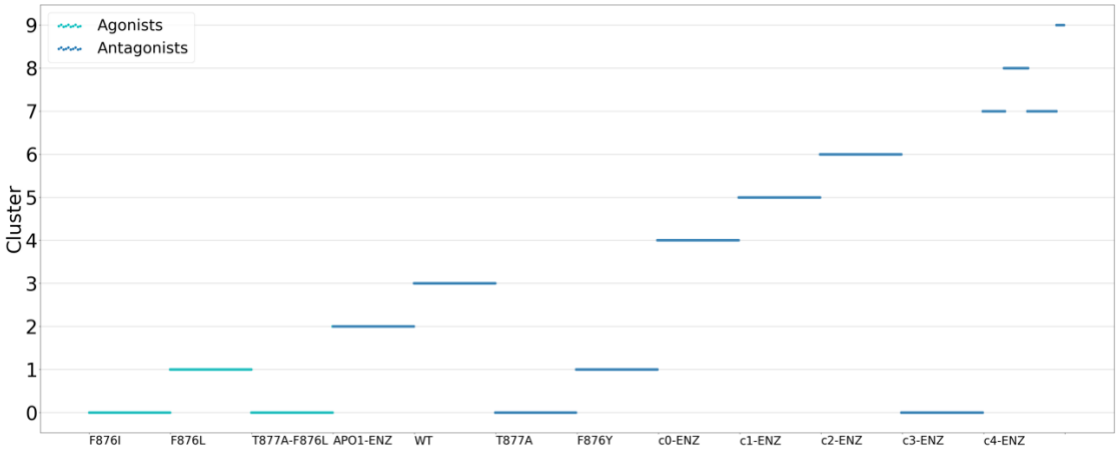

Figure 4.1 : Clustering of AR-ENZ simulations. Selected atoms: backbone excluding coils of the protein. Last 200ns of every simulation is considered.

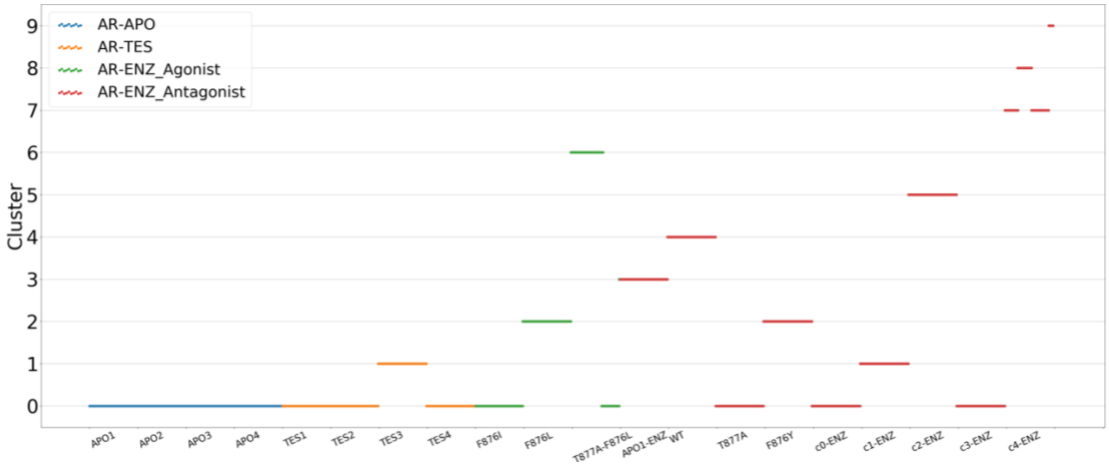

Figure 4.2 : Clustering of all of MD simulations. Selected atoms: backbone excluding coils of the protein. Last 200ns of every simulation is considered.

4.2. Cross Correlation Analysis

A cross-correlation analysis were considered in order to track movements of all residues in simulations. This analysis calculates movements of every residue in comparison with every other residue in the structure. Meanwhile, it shows if residues are correlated or not correlated to one another (Figure 4.3, and Figure 4.4).

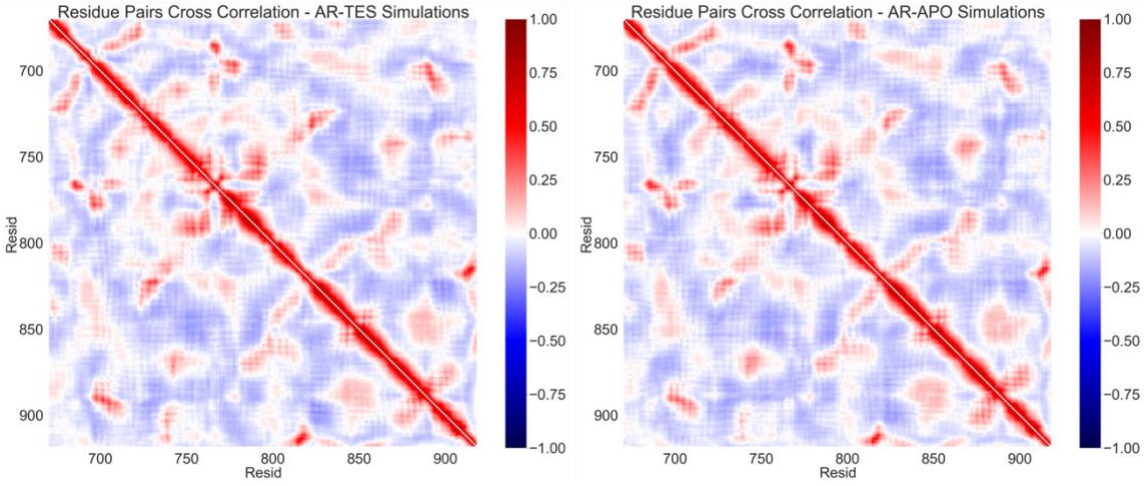

Figure 4.3 : Cross Correlation Analysis of AR-APO and AR-TES systems. Selected atoms: backbone. A value closer to 1 for a pair of residues means that they are correlated. However, a value closer to -1 shows that the pair of residues are anti-correlated.

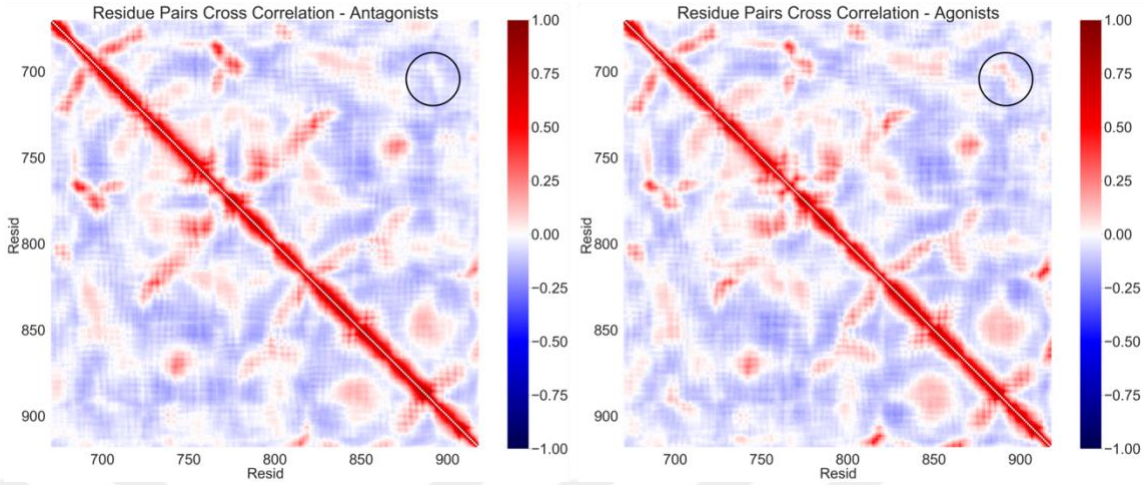

Figure 4.4 : Cross Correlation Analysis of AR-agonist and AR-antagonist systems. A value closer to 1 for a pair of residues means that they are correlated. However, a value closer to -1 shows that the pair of residues are anti-correlated. Selected: backbone atoms.

The most dominant difference is shown within black circles in Figure 4.4. The shown area correlates to regions of protein between residues 880 to 895, and 695 to 720. In other words, there is a correlation between these regions in agonist systems which is almost entirely absent in antagonist systems.

4.3. Principle Component Analysis (PCA)

PCA is a well-known technique for dimension reduction which is used in order to track conformation changes along simulations and observe similarities or differences among them. For PCA analysis, the first and second eigen-vectors (PC1 and PC2) were considered. According to simulation results, due to different conformations of H12 uopn antagonist binding, AR-antagonists simulations undergo different conformation changes compared to AR-agonist simulations (Figure 4.5). Moreover, a distinction could be considered between conformational changes in AR-APO, AR-TES, and AR-ENZ simulations (Figure 4.6).

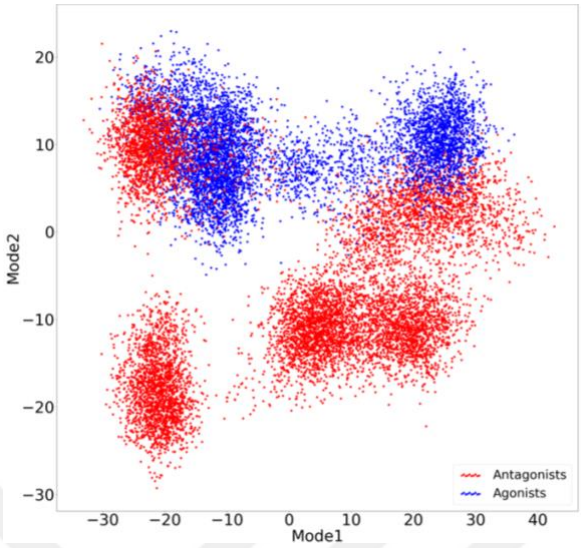

Figure 4.5 : PCA Analysis of AR-ENZ systems. Selected atoms: backbone, excluding coils of the protein. Last 200ns of every simulation is considered.

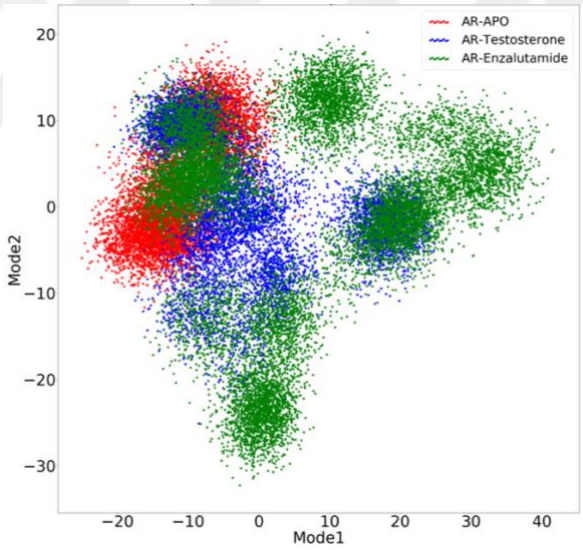

Figure 4.6 : PCA Analysis of All of MD simulations. Selected atoms: backbone, excluding coils of the protein. Last 200ns of every simulation is considered.

4.4. Root Mean Square Deviation (RMSD)

RMSD is a way of tracking how protein conformation changes in comparison to a reference structure which in this case, is the structure of protein in beginning of every simulation. Since loop regions in the protein fluctuate more and undergo bigger changes along a simulation, they were excluded in RMSD analysis.

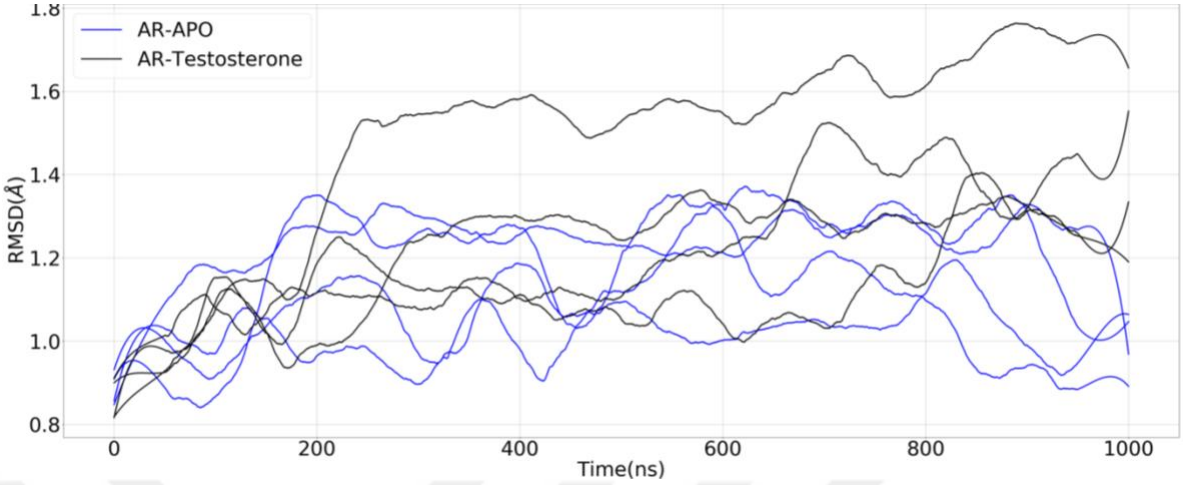

Figure 4.7 : RMSD of AR-APO and AR-TES simulations. Selected atoms: backbone, excluding coils of the protein.

Figure 4.7, shows that in general, there is a bigger conformation change in structures of AR-TES systems compared to AR-APO systems. Meanwhile, AR-APO systems are more stable.

There is not a significant difference between agonist and antagonist simulations (Figure 4.8). However according to Figure 4.9, there are fewer stable conformations in AR-ENZ systems compared to AR-APO or AR-TES systems.

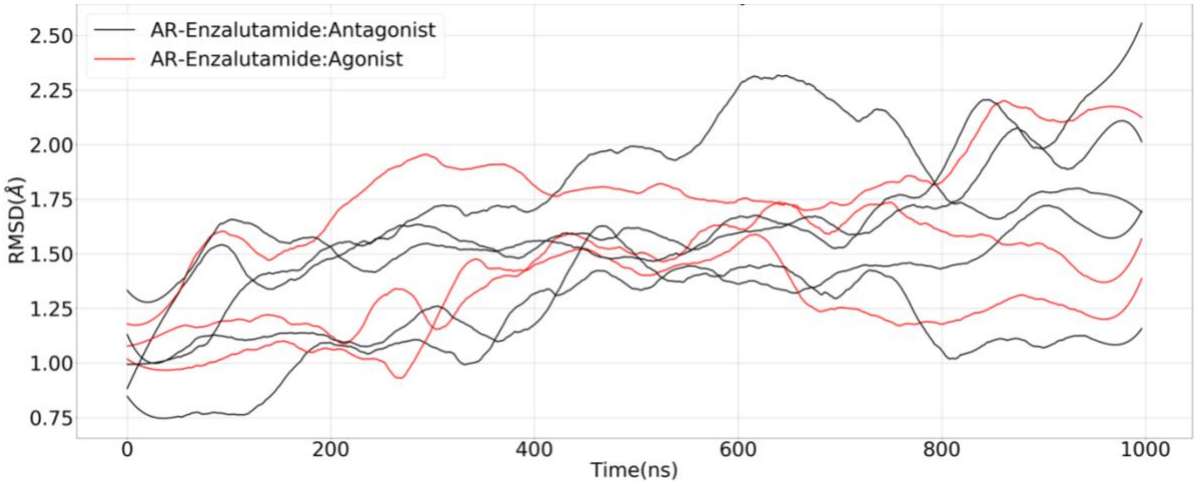

Figure 4.8 : RMSD of AR-ENZ simulations. Selected atoms: backbone, excluding coils of the protein.

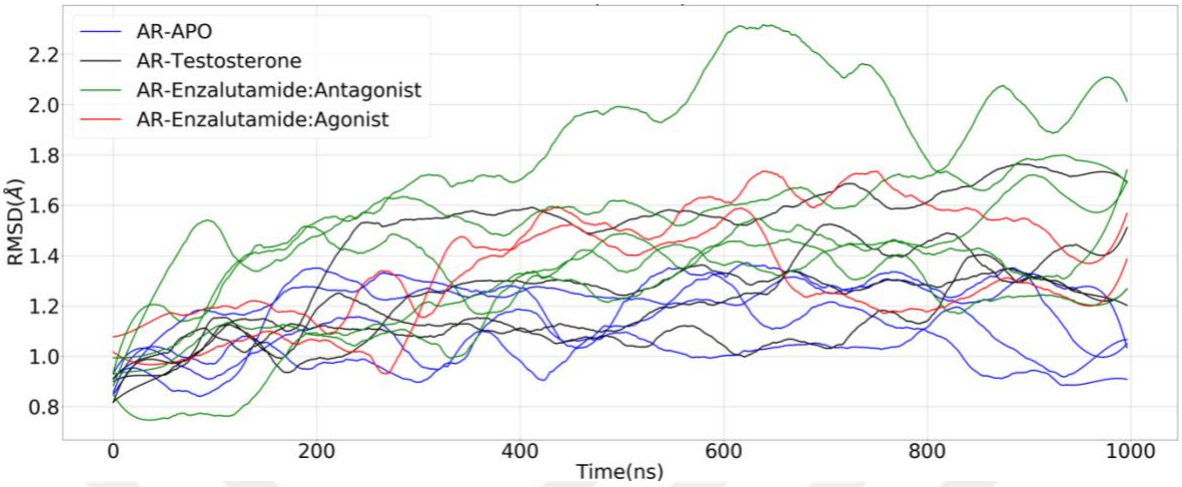

Figure 4.9 : RMSD of AR-APO, AR-TES, and AR-ENZ simulations. Selected atoms: backbone, excluding coils of the protein.

4.5. Root Mean Square Fluctuation (RMSF)

RMSF analysis were used with the aim of finding average fluctuations of residues in the protein along simulations. Figure 4.10, Figure 4.11, and Figure 4.12 are representations of RMSF results for all of AR-APO, AR-TES, and AR-ENZ simulations. Notice that helical regions of the protein are represented with gray background.

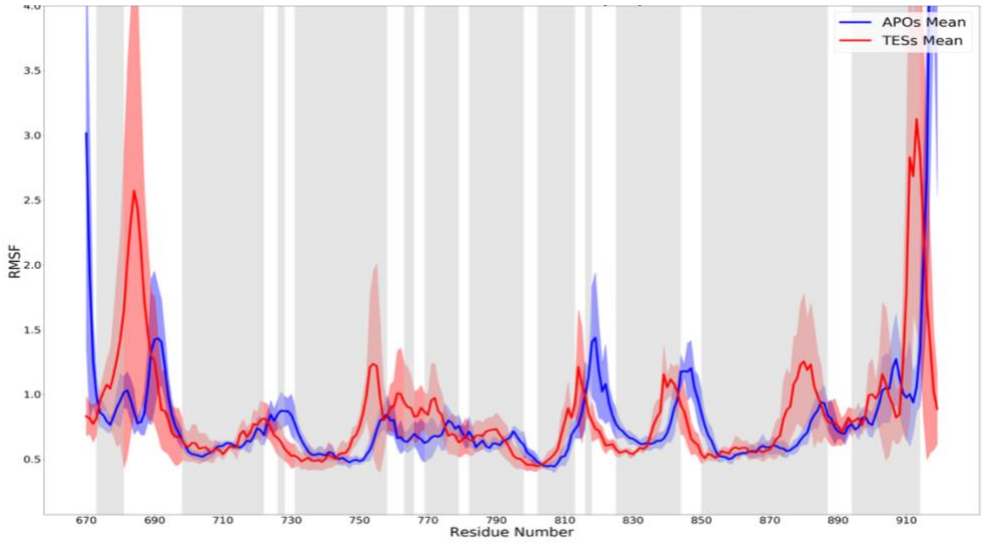

Figure 4.10 : RMSF of means of AR-APO systems and of AR-TES systems. Selected atoms: backbone. Standard deviations are shown in light blue and light red colors. Last 200ns of simulations are considered.

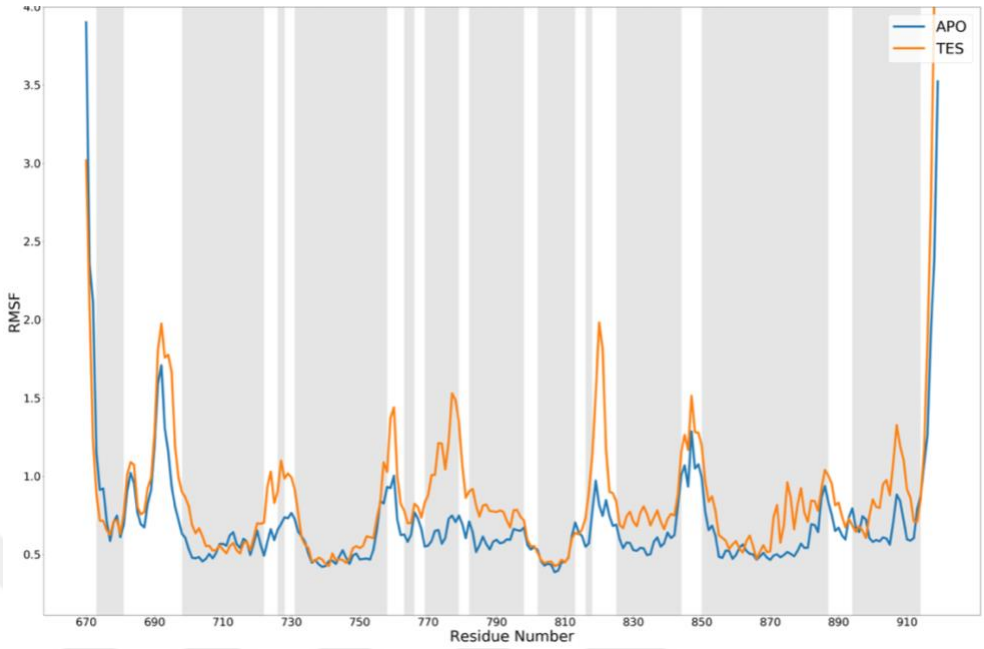

Figure 4.11 : RMSF of AR-APO-1 and AR-TES-1 Systems – 3 μs long simulations. Selected atoms: backbone. Last 200ns of simulations are considered.

The major difference according to cross-correlation analysis are shown within squares in Figure 4.12, and also, shown as protein segments in Figure 4.13.

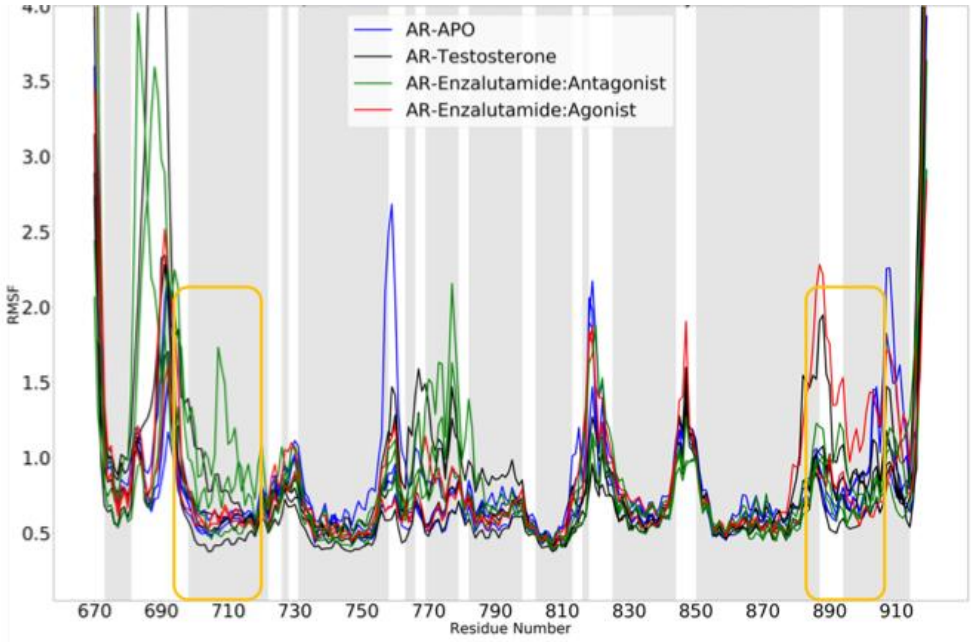

Figure 4.12 : RMSF of AR-APO, AR-TES, and AR-ENZ systems. Backbone atoms were considered. Last 200ns of simulations are considered.

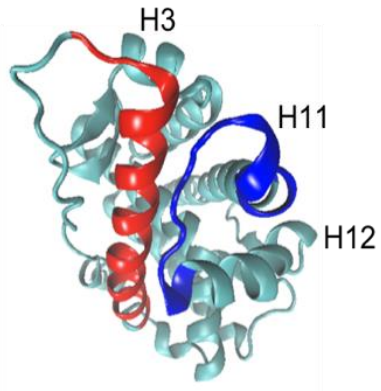

Figure 4.13 : Representation of residues 695-720 (a part of H3) in blue, and 880-895 (the loop and H11) in red.

Besides, superimposition of first clusters of AR-ENZ and AR-APO and AR-TES simulations shows a major difference in H3 and H11, as it is depicted in Figure 4.14.

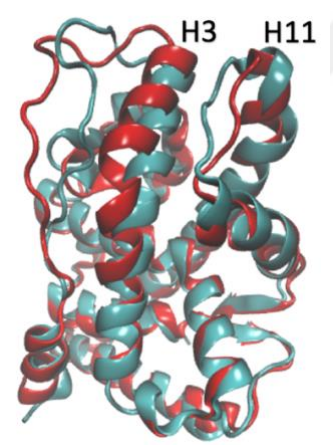

Figure 4.14 : Superimposition of the most dominant cluster of AR-APO, and, AR-TES systems' clustering results, with the most dominant cluster of AR-Enzalutamide systems' clustering results. structure in cyan shows the most dominant cluster of AR-APO and AR-Testosterone simulations, and structure in red shows the most dominant cluster correlating to AR-ENZ simulations.

5. ACCELERATED MOLECULAR DYNAMICS (AMD) SIMULATIONS

In General, during Classical MD (CMD) simulations the potential energy barriers are very high, thus systems typically fall in a local minima. In the case of this study, the AMD adds a total potential and an total dihedral energy to the actual potential and dihedral energies. Meanwhile, the height of local barriers are reduced by using this method. Setting parameters prior to AMD simulations is very important. Inaccurate parameters may lead to a low AMD simulation that can be the same as traditional MD simulation, or they may cause distortion in the protein (i.e. A helix could turn into a coil due to high energy levels in an AMD simulation).

In the current study, for preparation of parameters prior to AMD simulations, the structures after the first 100ns-long simulation of an AR-APO and an AR-TES were taken into account. Two types of parameters were considered as standard AMD parameters, and Fratev AMD parameters. [18]. We will name them AMD(S), and AMD(F), for simplicity. For AR-APO, and AR-TES systems, with every parameter type two replica simulations were run. Parameters for AMD(S) simulations were calculated using the equations 1, 2, 3, and 4.

$$E_{dihed} = \langle V_{dihed} \rangle + 4.n_{res} \tag{5.1}$$

$$\alpha_{dihed} = \frac{4}{5}.n_{res} \tag{5.2}$$

$$E_{total} = \langle V_{total} \rangle + \frac{n_{atom}}{5} \tag{5.3}$$

$$\alpha_{total} = \frac{n_{atom}}{5} \tag{5.4}$$

AMD(F) parameters however, were calculated via equations 5, 6, 7, and 8. It is worth to note that AMD(F) parameters have a lower acceleration rate compared to AMD(S) parameters.

$$E_{dihed} = \langle V_{dihed} \rangle + 3.5(n_{res}) \tag{5.5}$$

$$\alpha_{dihed} = \frac{E_{dihed}}{5} \tag{5.6}$$

$$E_{total} = \langle V_{total} \rangle + 0.16(n_{atom}) \tag{5.7}$$

$$\alpha_{total} = 0.16(n_{atom}) \tag{5.8}$$

5.1. Clustering Analysis

Similar to MD simulations, clustering analyses were done for all of AR-APO and AR-TES AMD simulations. As it is demonstrated in Figure 5.1 and Figure 5.2, AMD(S) simulations had different structure changes, and the protein took different conformations compared to CMD and or AMD(F) simulations.

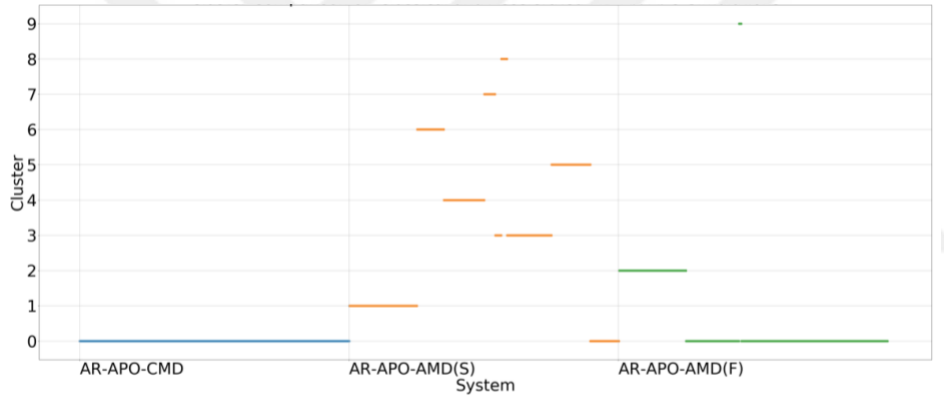

Figure 5.1 : Clustering of AR-APO AMD and CMD simulations. Selected atoms: backbone, excluding coils of the protein. Last 200 ns of each simulation is considered. Note that each color shows four simulation.

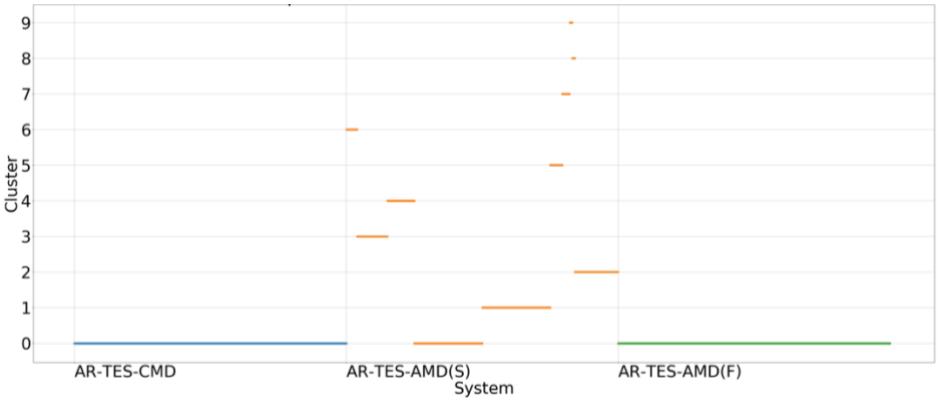

Figure 5.2 : Clustering of AR-TES AMD and CMD simulations. Selected atoms: backbone, excluding coils of the protein. Last 200 ns of each simulation is considered. Note that each color shows four simulation.

5.2. PCA

In order or to compare states and conformations that the protein acquires along different simulation systems, PCA was employed. PCA analysis showed that AMD(S) simulations had more difference in conformation change, compared to AMD(F), or CMD simulations (Figure 5.3, and Figure 5.4).

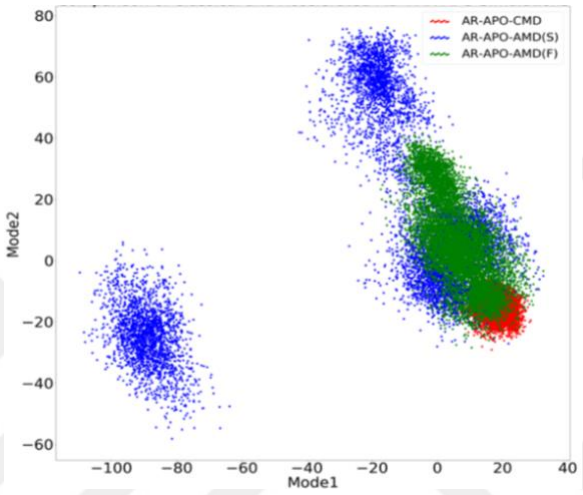

Figure 5.3 : PCA of all of AR-APO simulations. Selected atoms: backbone. The figure demonstrates how AMD simulations with Standard (S) parameters are majorly different, than those of classical MD or AMD with Fratev (F) parameters.

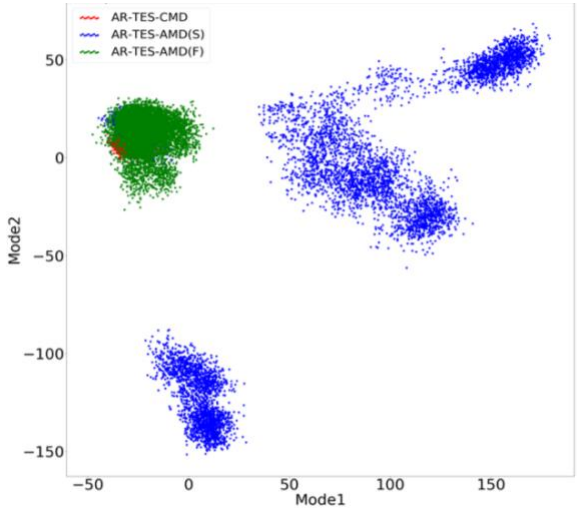

Figure 5.4 : PCA of all of AR-TES AMD and CMD simulations. Selected atoms: backbone. The figure demonstrates how AMD simulations with Standard (S) parameters are majorly different, than those of classical MD or AMD with Fratev (F) parameters.

5.3. Secondary Structure Analysis

Secondary structure analysis was utilized in order to find average helicity percentages for residues in all of simulation systems. Results of this analysis suggested that, there was a considerable helicity loss in H1, as shown in Figure 5.5.

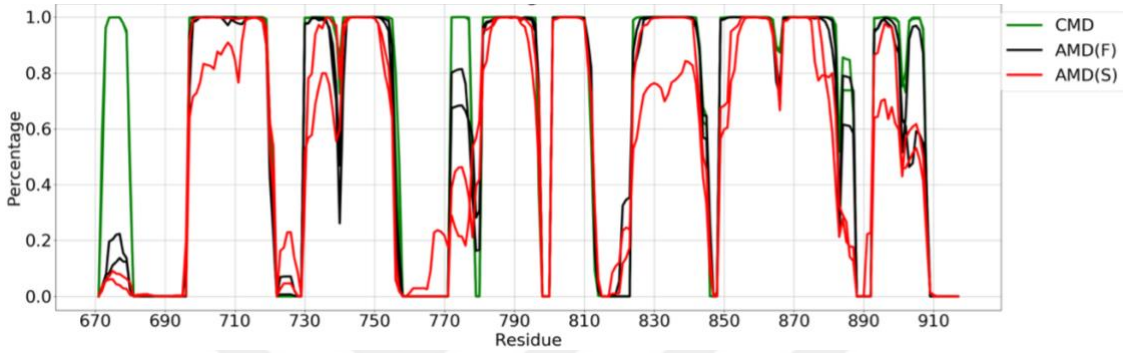

Figure 5.5 : Secondary structure analysis (helicity percentage) of all AR-APO-AMD and AR-TES-AMD simulations.

5.4. RMSD

RMSD analysis results of AMD simulations are demonstrated in Figure 5.6. Similar to PCA and clustering analyses results, according to RMSD analysis AMD(S) simulations have major difference in RMSD comparing to AMD(F) simulations. Specifically in AR-TES AMD simulations, RMSD values of AMD(S) are significantly higher than MD(F). In other words, in AMD(S) simulations, bigger conformation changes appear.

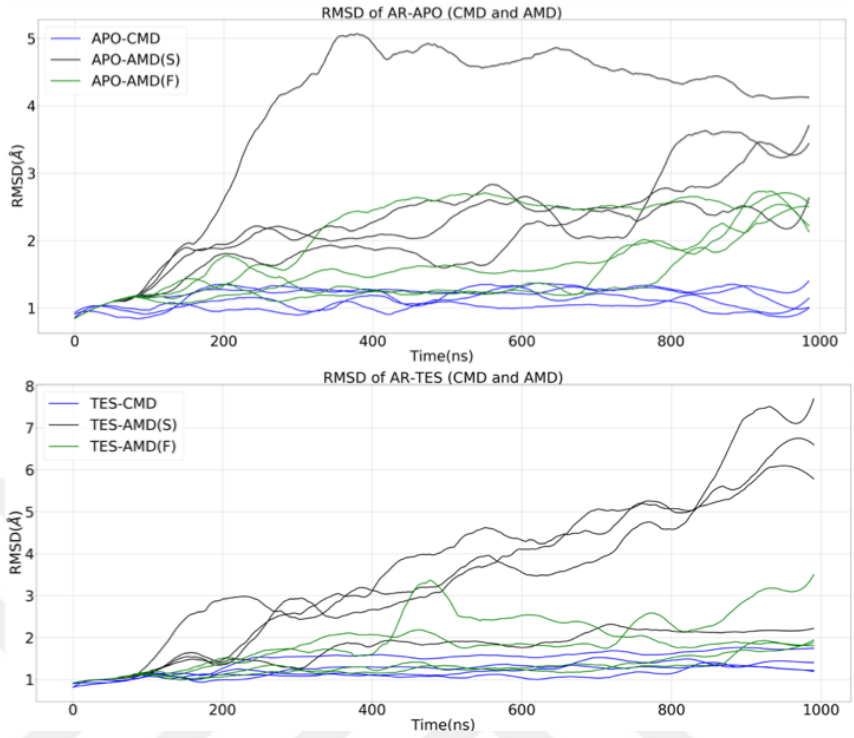

Figure 5.6 : RMSD of AR-APO and AR-TES AMD and CMD simulations. Selected atoms: backbone, excluding coils. Deviation of AMD simulations with Standard (S) parameters are higher than those of CMD or AMD with Fratev (F) simulations.

5.5. Re-run of AMD Simulations

After these results, only AMD simulations with Fratev parameters were considered as they had more stability. However, due to loss of helicity in H1 (residues 672 to 681), all of AMD simulations were run again. Meanwhile, after a couple of hundred nanoseconds in a MD simulation, H1 gradually becomes a coil. This can be a matter of critical change in structure of the protein. Thus, simulation trials considering three approaches with three kinds of constraints on H1, were run in order to keep H1 as a helix. The mentioned approaches are presented below.

1. In order to preserve the helicity of H1, the first method was to accelerate AMD simulations with a lower speed.

2. As a second method, a RMSD constraint was utilized for H1. The RMSD constraint was used to prevent the helix from losing its helicity, by keeping RMSD of atoms in the helix in a certain range.

3. Third method was to put a force constraint to keep pairs of alpha-carbons in a constant distant, thus keeping the helix as a helix (Figure 5.7).

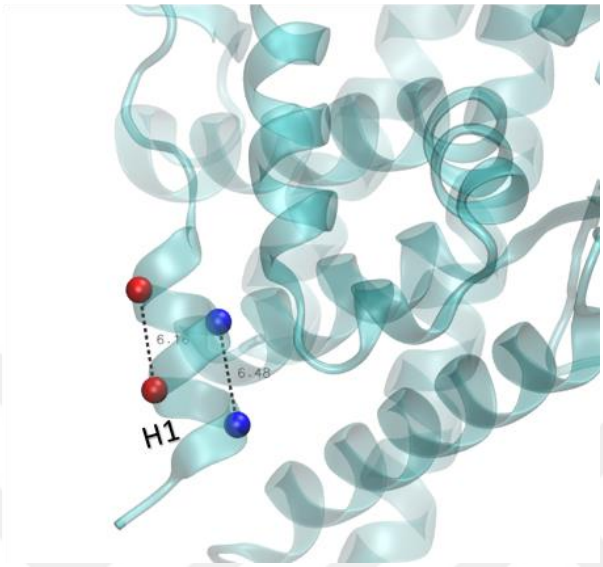

Figure 5.7 : Distance constant as a successful method in avoiding helicity loss in H1.

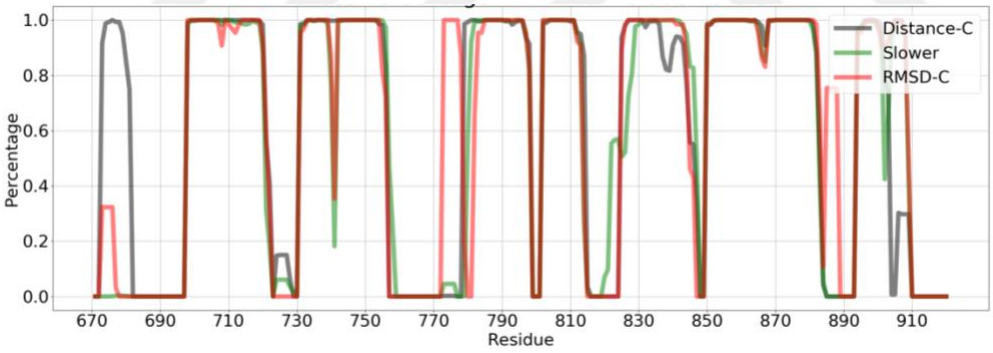

Figure 5.8 : Helicity percentage in three trials for AMD simulations.

The results of methods that we, are depicted in Figure 5.8. In it noteworthy to mention that, helicity of H1 was preserved utilizing the mentioned third method (Distance-C in Figure 5.8). Thus, we used this method in order to re-run all of the simulations. Figure 5.9, demonstrates a secondary structure analysis of the new AR-AMD simulations.

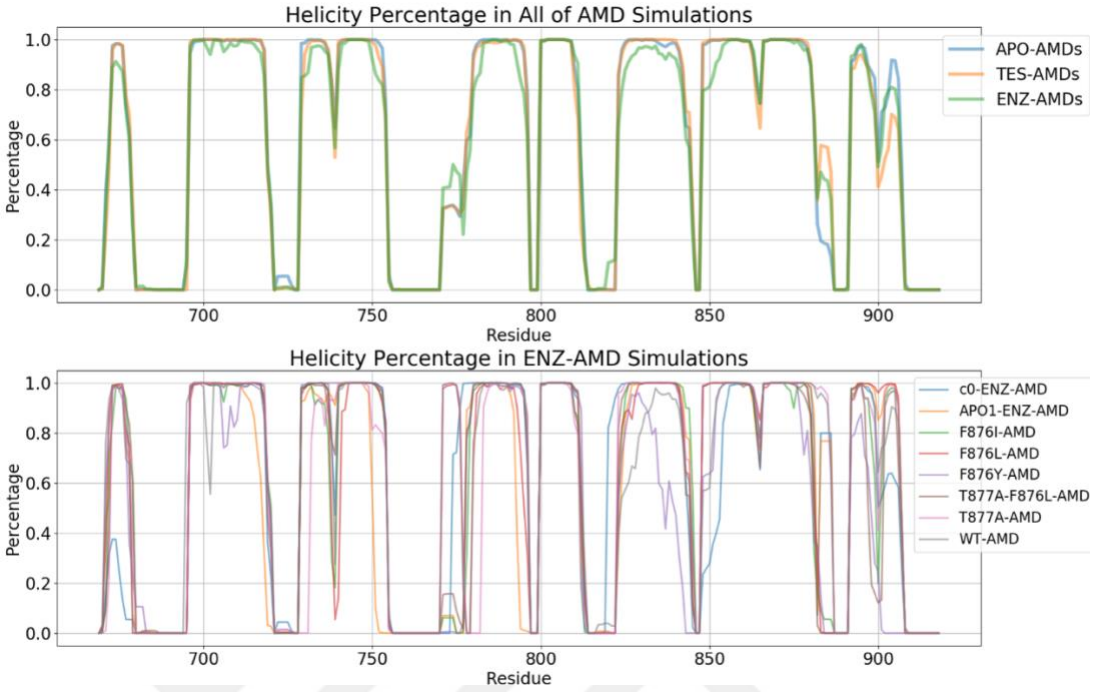

Figure 5.9 : Secondary structure analysis of Re-run AMD simulations.

6. ANALYSES FOR DYNAMICS OF THE REGION AROUND H11

6.1. Bend in H11

In this stage of study, for all of twelve AR-ENZ systems two more replicas were run to investigate more on the region around H11. As mentioned earlier, the area in cross-correlation analysis correlates to residues 695-720, and 880-895. By visual inspection of trajectories and tracking conformational changes in H11 the conclusion was that, in natural conformation of AR there is a bend in H11 (residues 883-888). For some simulations, the mentioned bend changed into a straight helix and thus, more focus on this helix was given. Figure 6.1 is a depiction of this bend in H11.

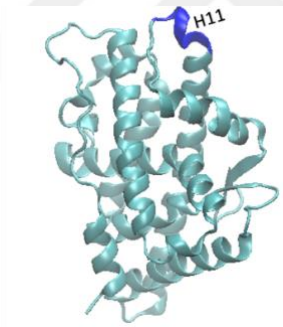

Figure 6.1 : The bend in H11: residues 883-888.

Furthermore, the bend and its transformation to the NotBend state was analyzed by tracking the distance between two alpha carbons on H11 (882I, and 886M) (Figure 6.2), along all simulations (Figure 6.3, Figure 6.4).

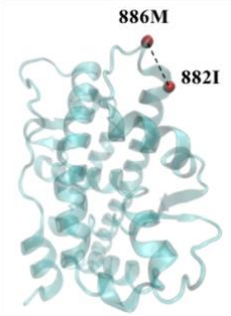

Figure 6.2 : 882I-886M distance for tracking the bend.

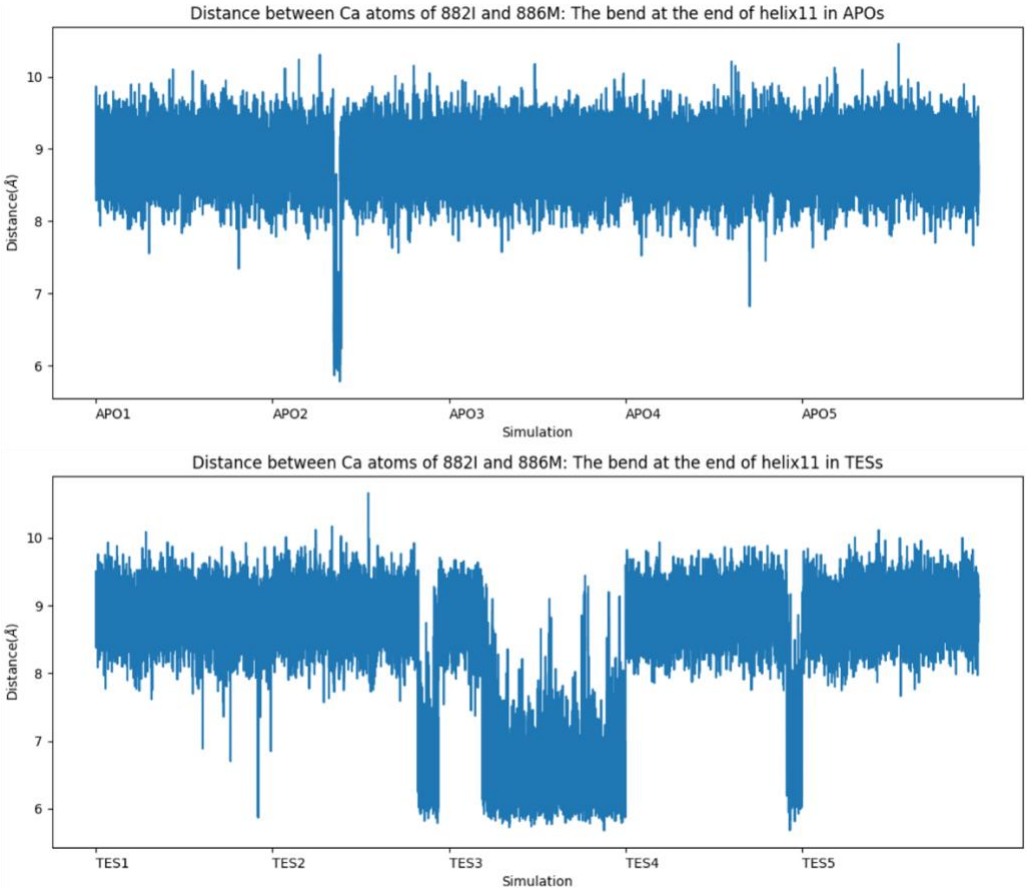

Figure 6.3 : Bend in AR-APO and AR-TES simulations. Distance between two alpha carbons of residues 882I, and 886M in H11 is considered to track the bend.

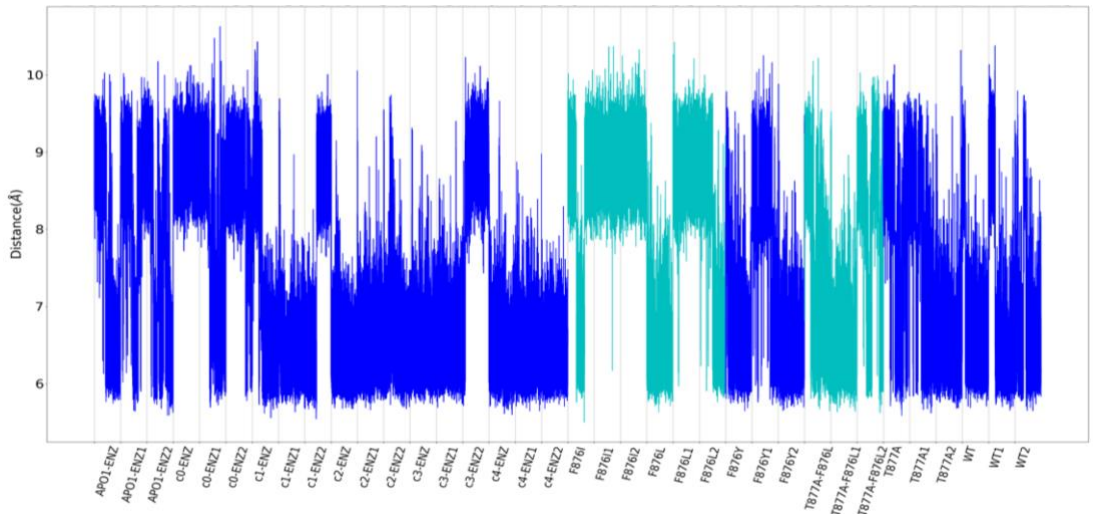

Figure 6.4 : Bend in AR-ENZ simulations. Replica simulations of AR-ENZ systems are included. Distance between two alpha carbons of residues 882I, and 886M in H11 is considered to track the bend. Antagonist systems are shown in blue, whereas agonist systems are shown in cyan.

The NotBend state is also seen in AR-APO and AR-TES systems, however, it is mostly seen in AR-ENZ systems.

Figure 6.5 is a depiction of states of the bend in H11 along AMD simulations. There is a correlation in AR-ENZ simulations between being an AR-Agonist and having the bend in H11, or otherwise, being an AR-Antagonist and the loss of the bend in H11.

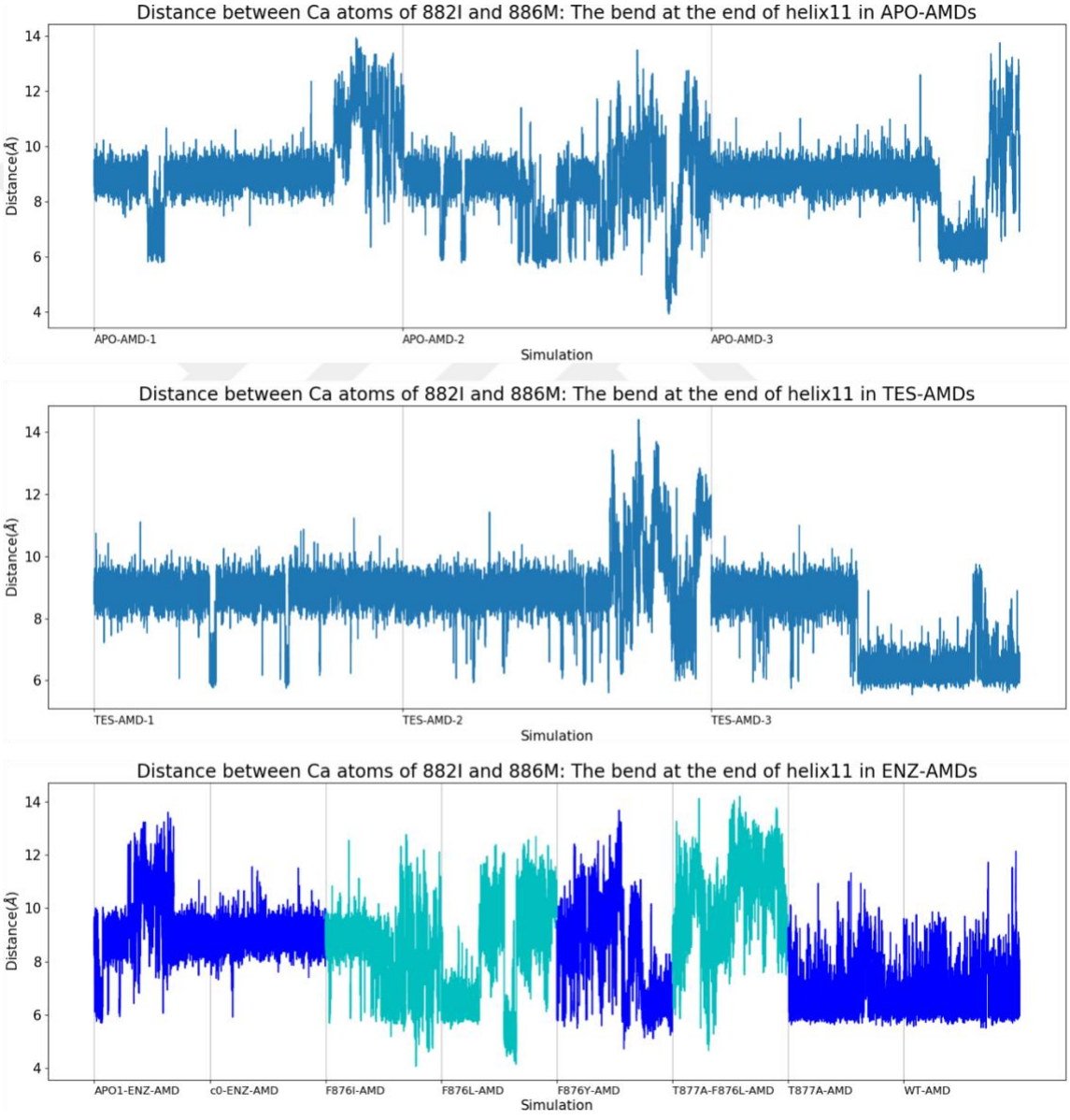

Figure 6.5 : Distance between two alpha carbons of residues 882I, and 886M for tracking the bend in all of AMD simulations. Antagonist systems are shown in blue, where agonist systems are shown in cyan.

It is noteworthy to mention that in none of the crystal structures in PDB bank, the NotBend state of H11 were seen. However, it appeared repeatedly in AR-ENZ simulations (Figure 6.6).

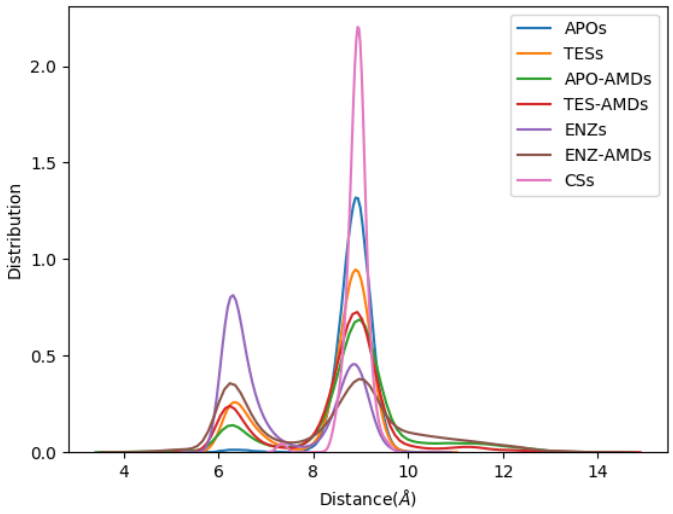

Figure 6.6 : Distribution of distance between residues 882I, and 886M for all of CMD and AMD simulations and for all available crystal structures in PDB bank.

These results suggested that, ENZ binding triggers H11 to lose its bend and become a more straight helix along with H10. Figure 6.7 is a superimposition of a bend and NotBend states of H11, in which the straightened helix is shown within red circle. Also, the conformation change of H12 is shown within yellow circle. In order to investigate more on the issue, all frames of all simulations were separated into two categories of Bend and NotBend frames.

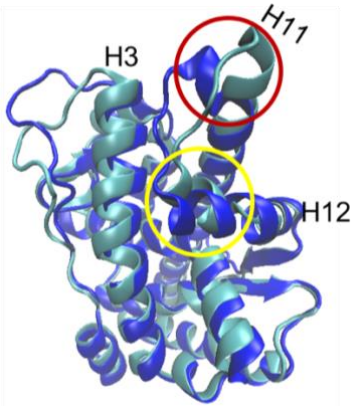

Figure 6.7 : Superimposition of two states with and without the bend in H11. Bend in Blue, and NotBend in cyan.

RMSF analysis of the separated frames as Bend and NotBend, is depicted in Figure 6.8. The blue region in AR in right side of Figure 6.8 correlates to the single beta-sheet which is present in the structure of AR. Generally this region fluctuate more upon ligand binding.

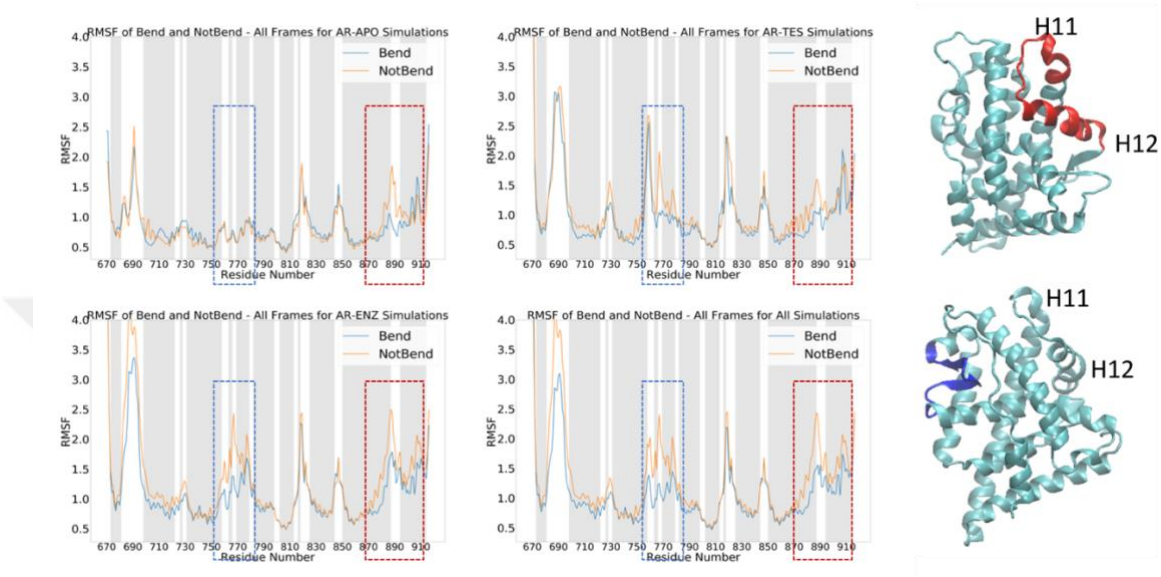

Figure 6.8 : RMSF of all bend and NotBend frames for all MD simulations.

A conclusion would be that, the mentioned residues on H11 and H12 in NotBend frames fluctuate more than those in Bend.

6.2. Tilt Angle in H3

Tilt angle of H3, suggests a different conformation of H3 in Bend and NotBend states, as it was demonstrated in Figure 4.14. NotBend state of H11 leads to more/stronger interactions between H10 and H3, and as a result brings H3 closer to H10 (Figure 6.9). This leads to fewer/weaker interactions between H10 and H12, which allows H12 to moves freely outside the LBP.

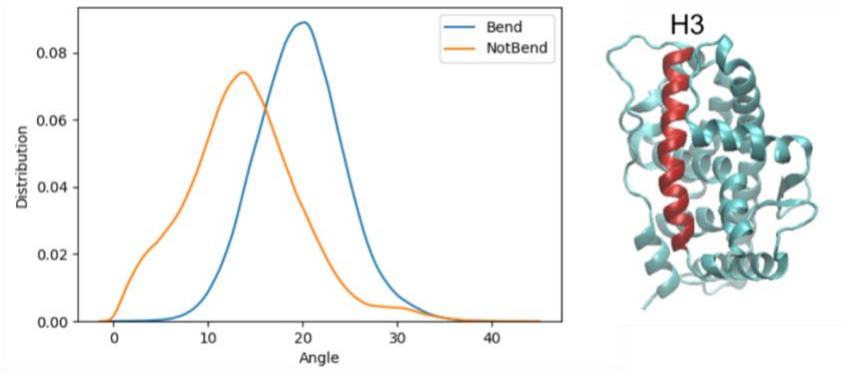

Figure 6.9 : Distribution of tilting angle of H3 next to a depiction of the helix in the protein structure.

6.3. Correlation Between Agonistic/Antagonistic Activity of Enzalutamide and the Bend/NotBend in H11

The results of 882I-886M distance analysis for all simulation suggested that, the Bend state correlates to agonist-binding and the NotBend state correlates to antagonist-binding as demonstrated in Figure 6.10. Moreover, upon antagonist binding the 882I-886M distance is decreased which leads to the NotBend state in H11.

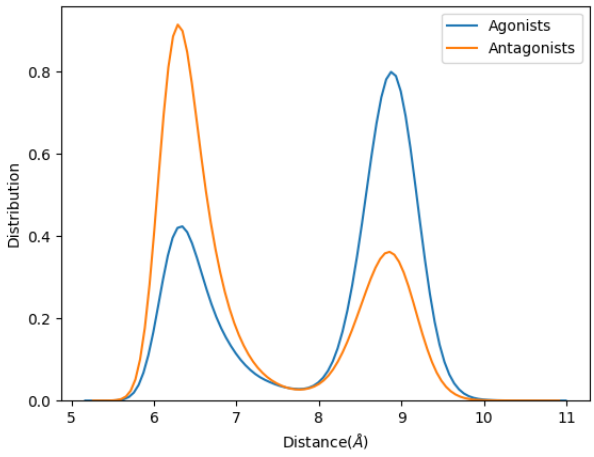

Figure 6.10 : Distribution of distance between residues 882I, and 886M upon Agonist and or Antagonist Binding.

6.4. Distance Based Analysis

For the purpose of tracking movement of critical segments around H11 and H12, distance analysis among these segments were done. According to Figure 6.11, Figure 6.12, and

Figure 6.13, after the transition of Bend to NotBend in H11, the loop between H11 and H12 moves from H10 and H3. Besides, H12 moves away from H3.

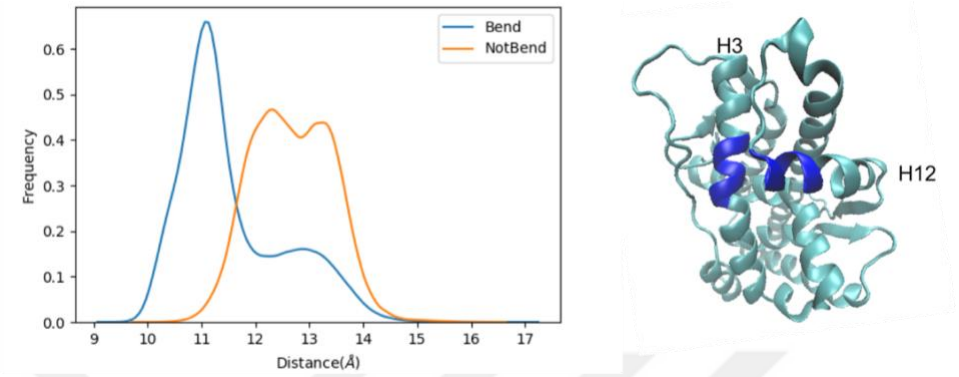

Figure 6.11 : Movement of H12 away from H3. Distance between 706-711 and 893-899.

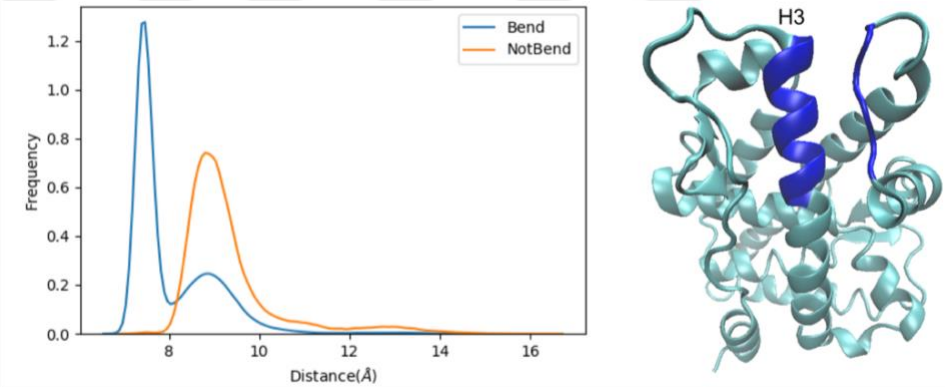

Figure 6.12 : Movement of loop away from H3. Distance between 698-708 and 888-892.

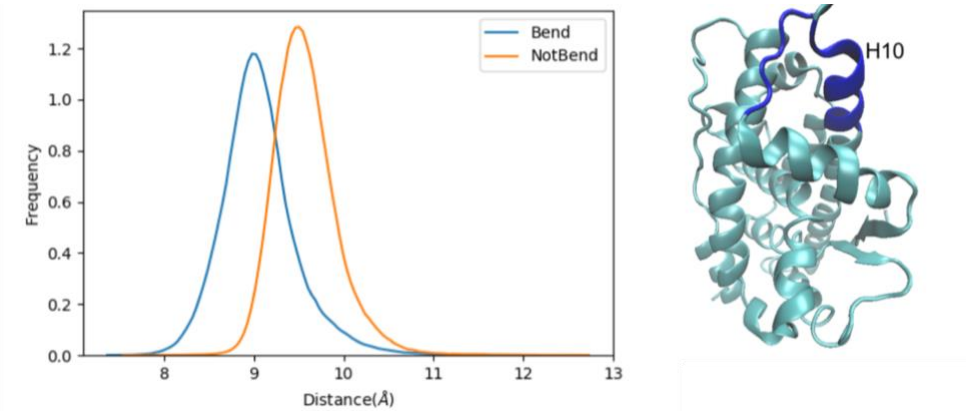

Figure 6.13 : Movement of loop away from H10. Distance between 876-885 and 888-892.

As shown in Figure 6.14, in AMD simulations also, there is the same behavior in H12, which moves away from H3.

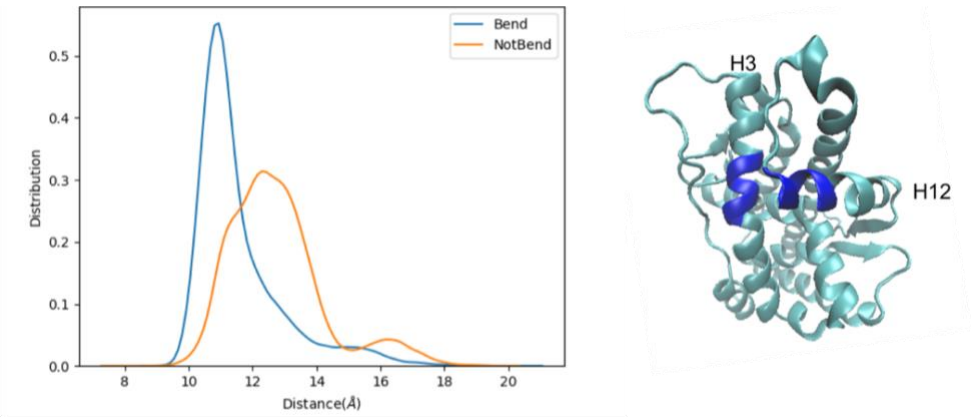

Figure 6.14 : Movement of H12 away from H3 in AMD simulations. Distance between 706-711 and 893-899.

Figure 6.15, is a depiction of how agonistic or antagonistic activity in AR affects the distance between H3 and H12. H12 is far away from H3 in those of AR-antagonist systems.

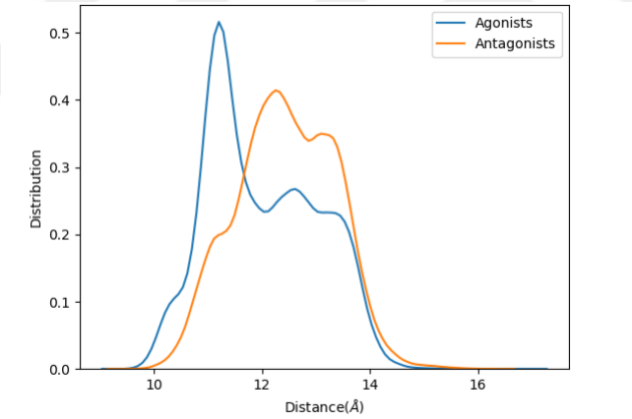

Figure 6.15 : Distribution of distance between H3 (706-711) and H12 (893-899) in agonistic and antagonistic AR-ENZ simulations.

6.5. Behavior of H12 According to PCA Analysis

PCA analysis as shown in Figure 6.16, also suggests conformation changes of H12, that differs in NotBend and Bend states. In other words, upon antagonist binding H12 undergoes a different conformation than upon agonist binding.

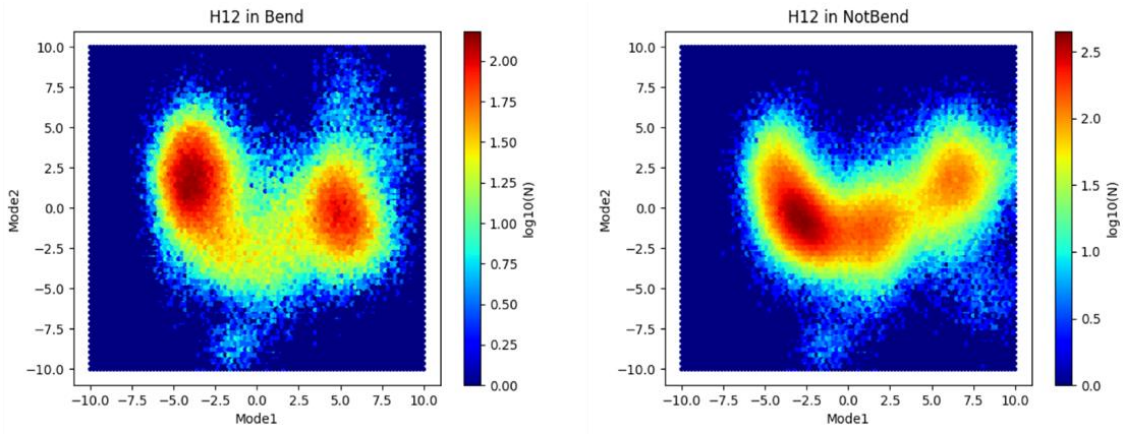

Figure 6.16 : PCA analysis of CMD simulations for H12: Behavior of H12 in Bend and NotBend.

Moreover, PCA analysis of Bend and NotBend frames for H12 in AMD simulations suggest slighter difference in conformation changes of H12 along the simulations (Figure 6.17).

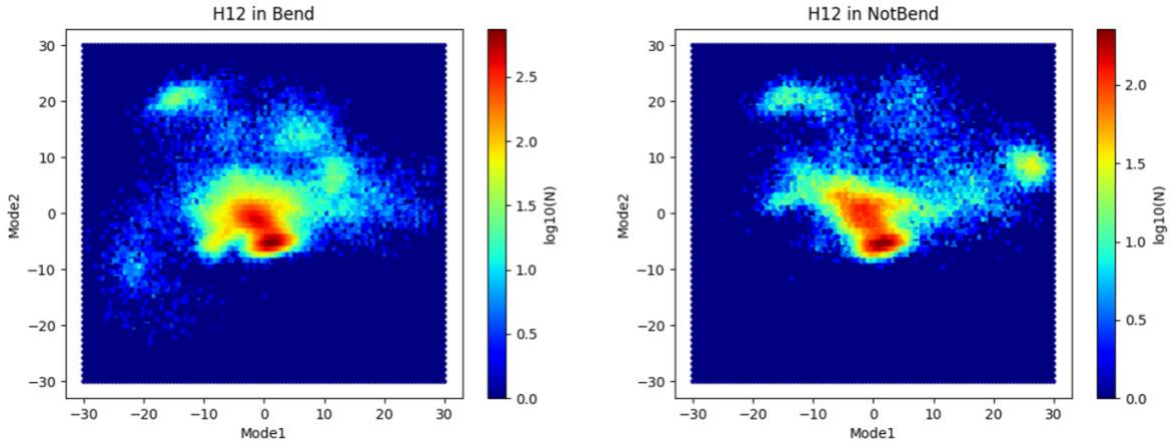

Figure 6.17 : PCA analysis of AMD simulations for H12: Behavior of H12 in Bend and NotBend.

6.6. Analysis of Effect of Straightened H11 on Movement of H12

According to the results from distance analyses, movement of H12 is correlated with Bend or NotBend state of H11. Our hypothesis states that unbending of H11 causes the movement of H12 away from H3. In order to validate this claim, MD simulations with modified protein structures were run. Three sets of simulations were considered to address this matter as follow.

6.6.1. Changing NotBend to Bend in a structure with NotBend-H11 state

For this simulation, a structure of the AR with NotBend-H11 was modified by changing it to Bend-H11, and 1μs-long simulation was run. According to distance analyses, changing NotBend to Bend, leads to less distance between H10 and the loop between H11 and H12. In other words, in the new structure this distance is closer to a structure with Bend-H11 (Figure 6.18). In the typical structure with NotBend-H11, the loop between H11 and H12 moves away from H3, and changing H11 to Bend state, dose not bring the loop closer to H3, as it is the case in the typical structure with Bend-H11 (Figure 6.19). According to Figure 6.11 and Figure 6.14, in the typical structure with NotBend-H11, H12 moves away from H3. This change in structure of the protein does not return to its position in Bend state, upon modifying the structure with NotBend-11 (Figure 6.20).

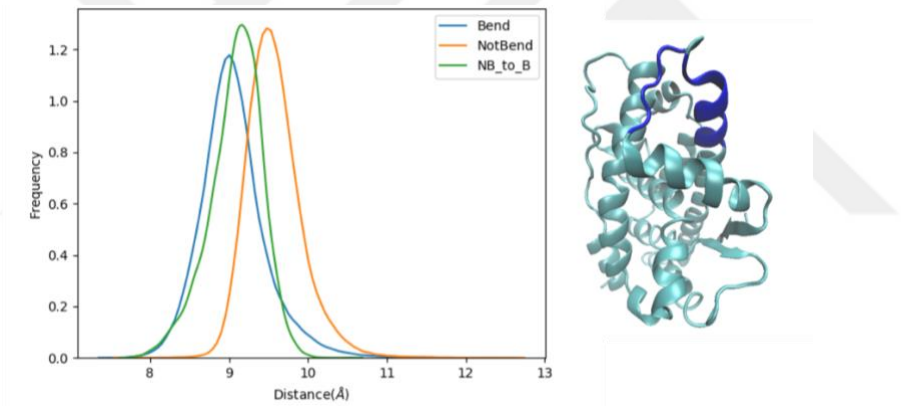

Figure 6.18 : Distance between H10 (876-885) and the loop (888-892) - NotBend to Bend.

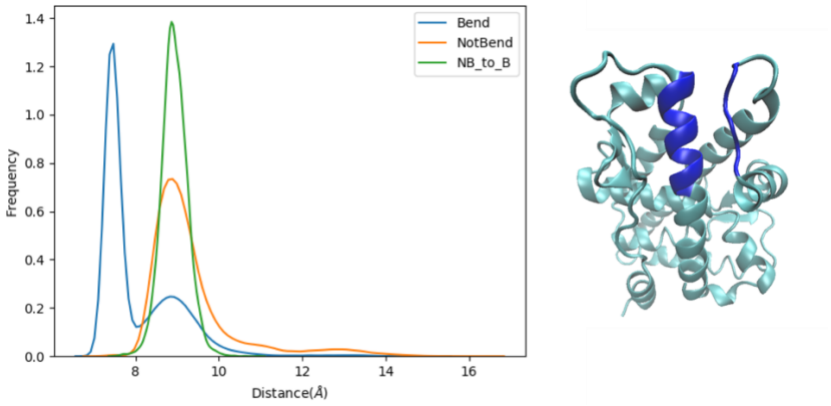

Figure 6.19 : Distance between H3 (698-708) and the loop (888-892) - NotBend to Bend.

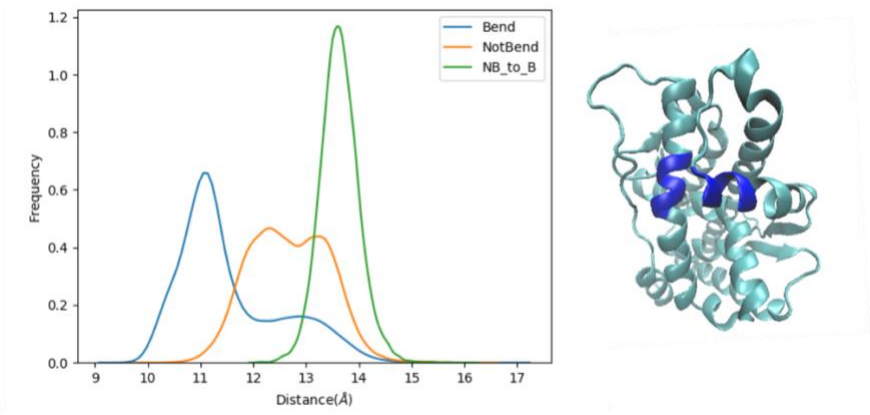

Figure 6.20 : Distance between H3 (706-711) and H12 (893-899) - NotBend to Bend.

6.6.2. Changing Bend to NotBend in a structure with Bend-H11 state

Similarly, the Bend state of a AR was modified to NotBend state. After analyzing the simulation results, the conclusion was that changing Bend to NotBend leads in more distance between H10 and the loop between H11 and H12. This suggests that, the new structure is similar to a structure with typical NotBend-H11 (Figure 6.21). The distance between H3 and the loop also increases upon this change (Figure 6.22). More importantly, due to this arbitrary change, H12 moves away from H12 (Figure 6.23).

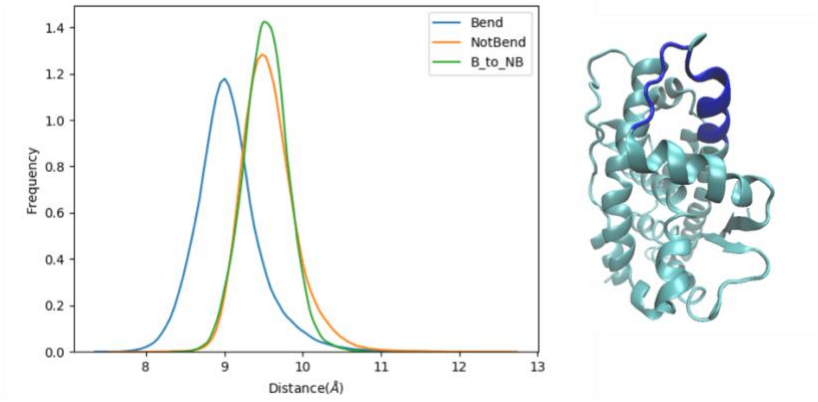

Figure 6.21 : Distance between H10 (876-885) and the loop (888-892) - Bend to NotBend.

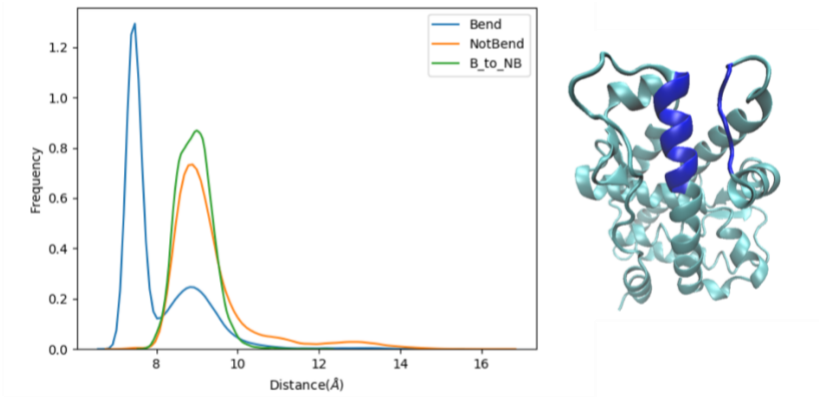

Figure 6.22 : Distance between H3 (698-708) and the loop (888-892) - Bend to NotBend.

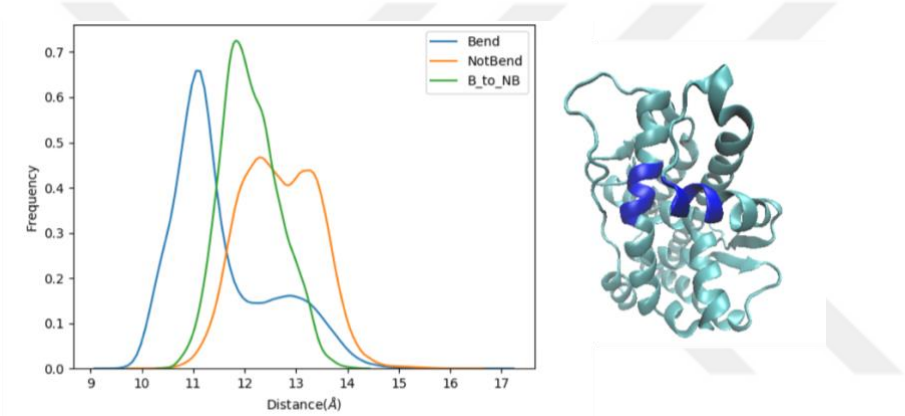

Figure 6.23 : Distance between H3 (706-711) and H12 (893-899) - Bend to NotBend.

6.6.3. Pulling the loop between H11 and H12 away from H10 and H3

In this approach, the loop was pulled away from H10 and H3, and a force was applied to keep it away from H3 and H11 along the simulation. In order to do this, distances of residue pairs between H3 and the loop, and H10 and the loop were forced to stay in certain distances. H11 also was fixed in Bend state, using distance force constraints. In this case, Figure 6.24 and Figure 6.25 show that the loop was kept in the predefined distance away from H3 and H10 along the simulation. Figure 6.26 demonstrates that pulling the loop away from H10 and H3, leads to loss of interactions between the loop between H11 and H12, and H3 or H10. H12 is more free due to a free neighboring coil, thus it could move away from LBP.

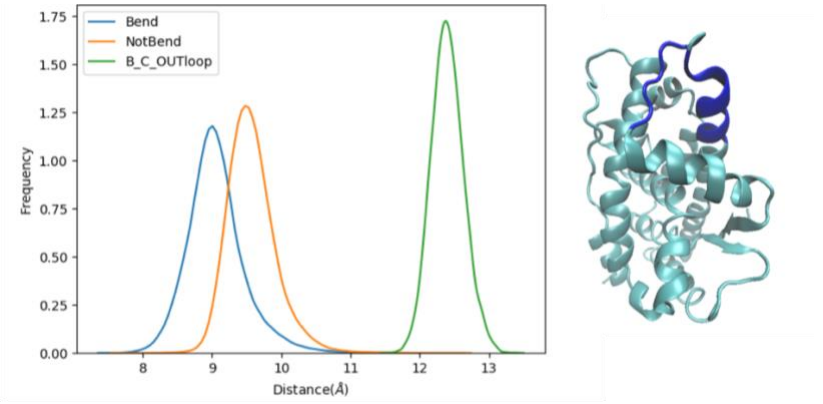

Figure 6.24 : Distance between H10 (876-885) and the loop (888-892) - Pulling the loop away from H3 and H12.

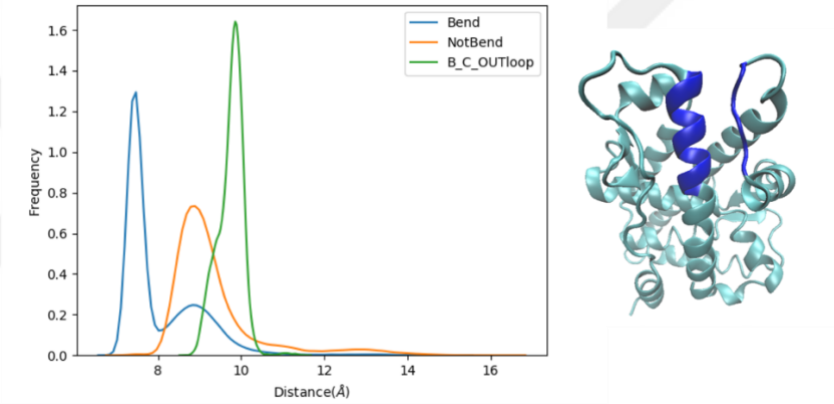

Figure 6.25 : Distance between H3 (698-708) and the loop (888-892) - Pulling the loop away from H3 and H12.

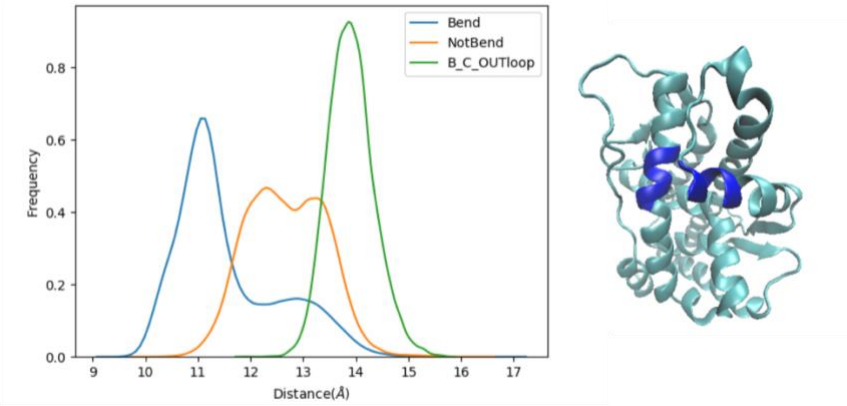

Figure 6.26 : Distance between H3 (706-711) and H12 (893-899) - Pulling the loop away from H3 and H12.

6.7. A Network Based on Residue Pair Distance

A novel approach was considered in order to presumably build a network of intramolecular interactions based on distances of residue pairs. As mentioned earlier, frames of all simulation, were separated into two categories of Bend and NotBend, based on the distance between residues 882I and 886M. Assuming that a residue pair in a distance less than 6.5Å would interact, a cut-off of 6.5 Å was considered. For every simulation, a matrix (250x250) was constructed, in which for each pair of residues, percentage of interactions along the simulations was included. Further on, two distinct networks of interactions were considered for Bend and NotBend frames. Figure 6.27 demonstrates the most dominant difference in these two networks in regions around the bend in H11.

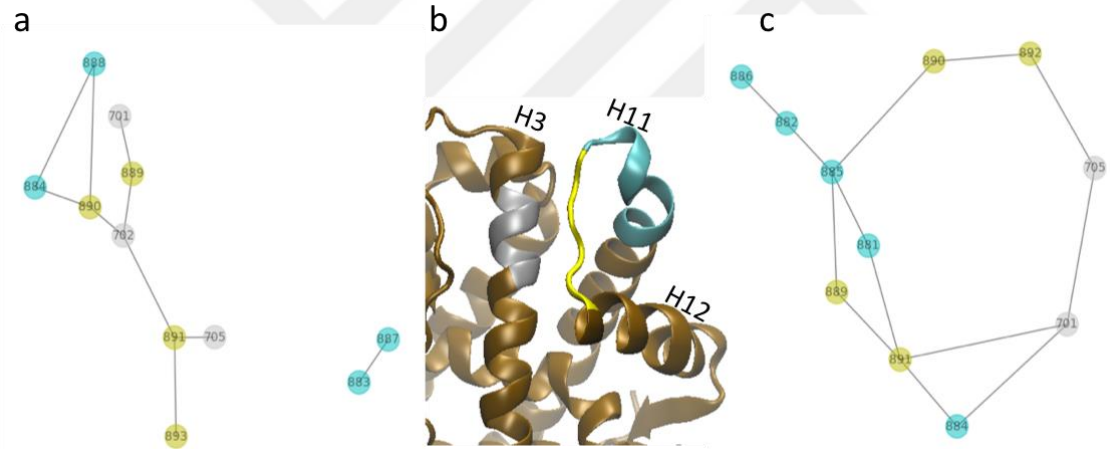

Figure 6.27 : Residue networks based on their alpha carbon distance, built for Bend and NotBend frames of all MD simulations. Only residues in H11 and first part of H3 is considered. (a) shows the Bend, and (c) shows NotBend network.

This analysis suggests that, transition of Bend to NotBend happens as interaction between the loop between H11 and H12, and the first part of H3 breaks. This allows the mentioned loop (residues 889 to 893) to be free. Therefore, interaction between residue 891 and 895 and 896 breaks, and finally it leads to movement of H12 away from H3. Afterwards, residues 880 and 881 interact with residues 884-886, thus making H11 to be a straight helix along with H10.

6.8. Feature Selection Analysis

After interaction analysis using Pycontact and distance-based network analysis, in order to find a pathway from bend in H11 to H12, feature importance using random forest method was applied separately on interaction scores from Pycontact and distance-based network analyses. A matrix were built for all of simulations in which, rows of the matrix were consisted of the simulations names, and in columns residue numbers were included. Values in the matrix were average interaction scores between each residue and ENZ along every simulation. A target column with the name of "Straightened" was added to the matrix that could held values of 1 or 0, correlating to loss of bend or preservation of it in H11, respectively. Using feature importance by random forest, the most important residues were chosen. The hypothesis is that interactions of these residues with ENZ lead to the NotBend H11. Results suggested that, when residues 701, 704, 705, 708, 741, 742, 746, 764, 876, 877, 889, 890, 891, and 895 interact with enzalutamide, the result is loss of the bend in H11. Figure 6.28, is a depiction of the mentioned residues in the protein structure.

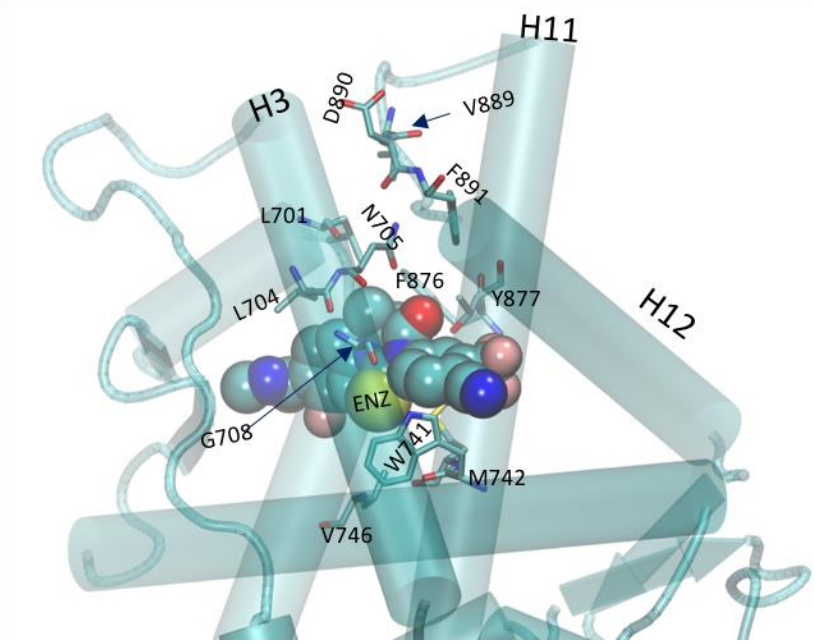

Figure 6.28 : Important residues interacting with ENZ that make H11 to lose its bend.

Another similar feature selection analysis were conducted in which the columns were residue pairs. Considering the results of this analysis, intramolecular interactions that lead

to the NotBend H11 upon ENZ binding were identified. According to the our feature selection results, upon ENZ binding the following interaction pathway leads to loss of bend in H11.

1. Enzalutamide interacts with LEU701, and weakens/breaks interactions between LEU701, and VAL889.

   Enzalutamide interacts with ASN705, and weakens/breaks interactions between ASN705 and ASP890, and between ASN705 and PHE891.
2. LEU880-PHE891 interaction breaks or weakens. This leads to freedom of the loop between H11 and H12.
3. LEU880 interacts with LEU701 and probably ASN705 (Figure 6.29), thus H10 becomes closers to H3 and the this leads to loss of bend in H11. 880-884, 881-885 interactions occur/become stronger. This also explains the tilting angle of H3 that is smaller upon antagonist-binding (NotBend state in Figure 6.9). In other words, when H10 becomes closer to H3, H3 is much straighter.
4. As a result, the loop between H11 and H12 is free and moves outside the ligand binding pocket, thus freeing H12 to move away from ligand binding pocket. A depiction of mentioned pathway is depicted in Figure 6.30.

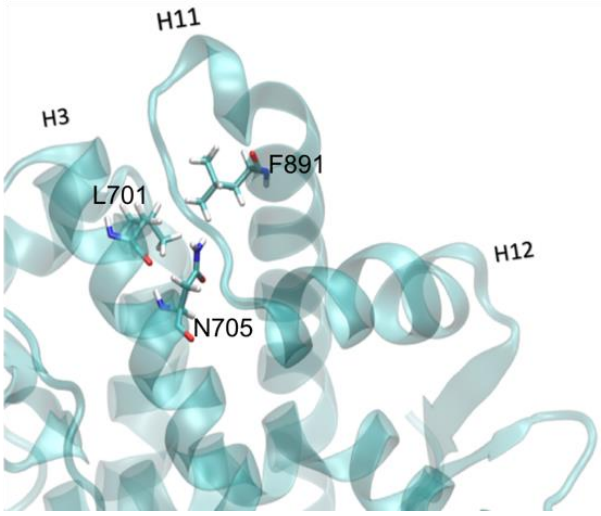

Figure 6.29 : Interaction of residues LEU880, LEU701, and ASN705.

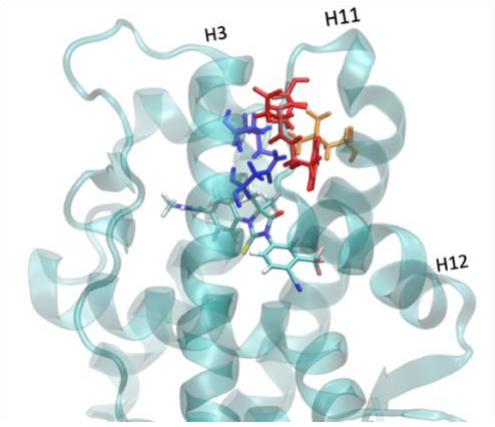

Figure 6.30 : Pathway of Bend to NotBend; 1. Enzalutamide interacts with residues in blue. 2. Interactions between residues in blue and residues in red breaks or becomes weak. 3. Interaction between residues in red and residue in orange breaks. 4. Residue in orange, and residues in blue interact.

6.9. Finding the Pathway

Results of interaction analysis using Pycontact on H3, H11, and the loop between H11 and H12 are shown in Figure 6.31. Note that loss of interactions between the loop and H3 or H10 is visible.

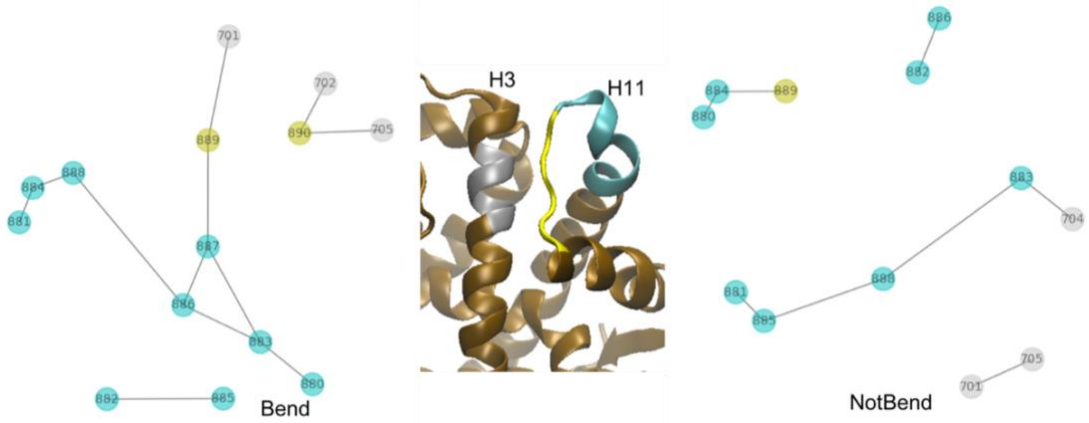

Figure 6.31 : Interaction network based on Interactions analysis from Pycontact among H3, H11, and the loop between H11 and H12.

Maps of intramolecular interactions according to distance based network are demonstrated in Figure 6.32. Loss of bend in H11 results in loss of interactions between H3 and the loop between H11 and H12, and finally results in more interactions between H10 and H11 making it a straight helix.

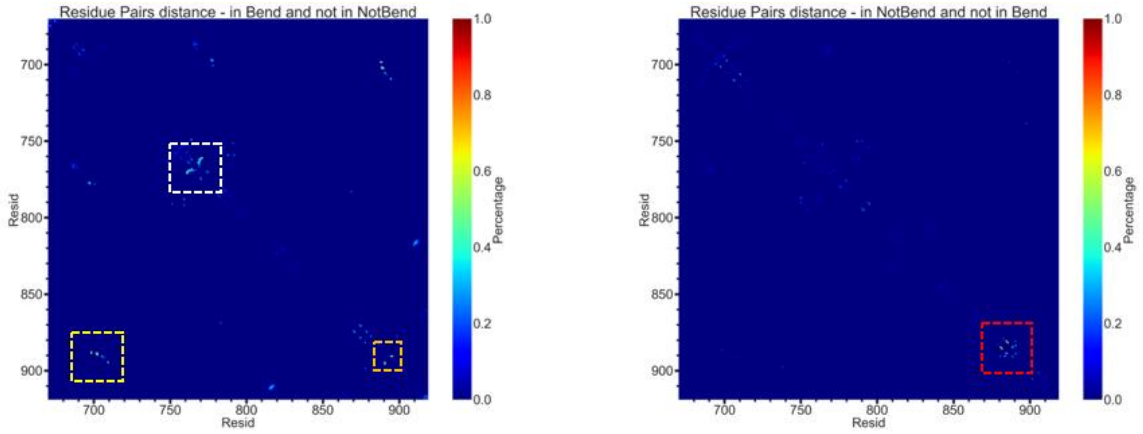

Figure 6.32 : Map of intramolecular interactions in all of CMD simulations; area within white square correlates to interactions in the only beta-sheet in the protein structure. Area within yellow square correlates to interactions between H3 and H11 together with the loop between H11 and H12. Finally, the area within orange and red squares correlate to interactions between H10 and H11, that shows there are more interactions in NotBend state, making H10 and H11 a single NotBend helix.

Figure 6.33, is a bar plot of hydrogen bond (h-bond) interactions between H3, the loop, and H11, and the mentioned key residue pair interaction (ASN705, and PHE891) is noticeable.

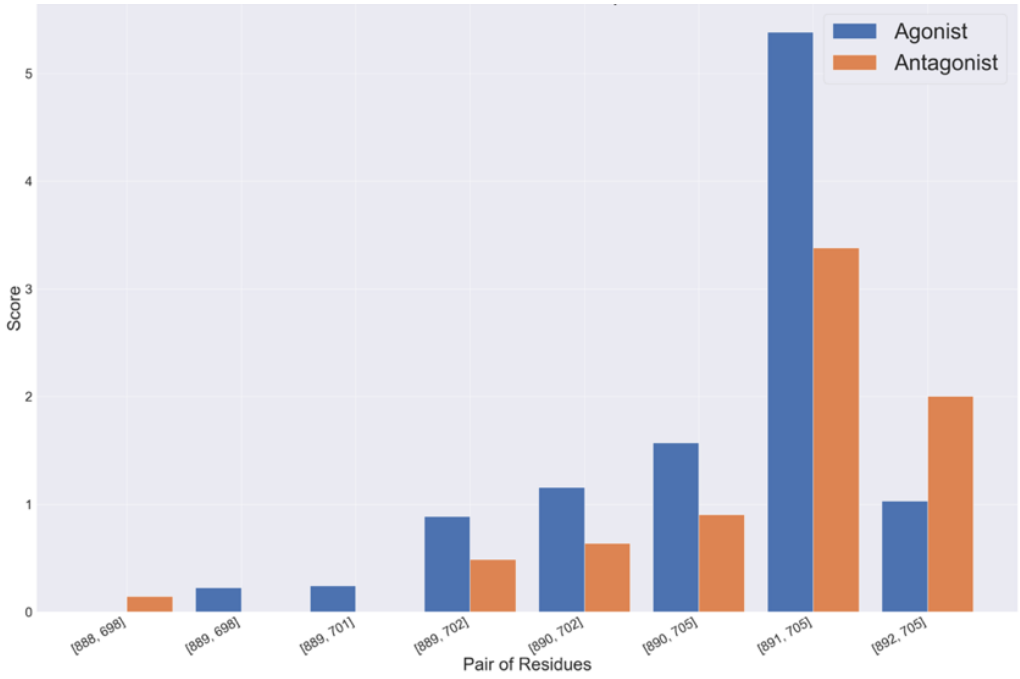

Figure 6.33 : Interactions among segments H3, H11, and the loop between H11 and H12 in CMD simulations.

In NotBend state, H10 comes closer to LBP, thus there is a h-bond interaction between SER884 and VAL889 (Figure 6.34).

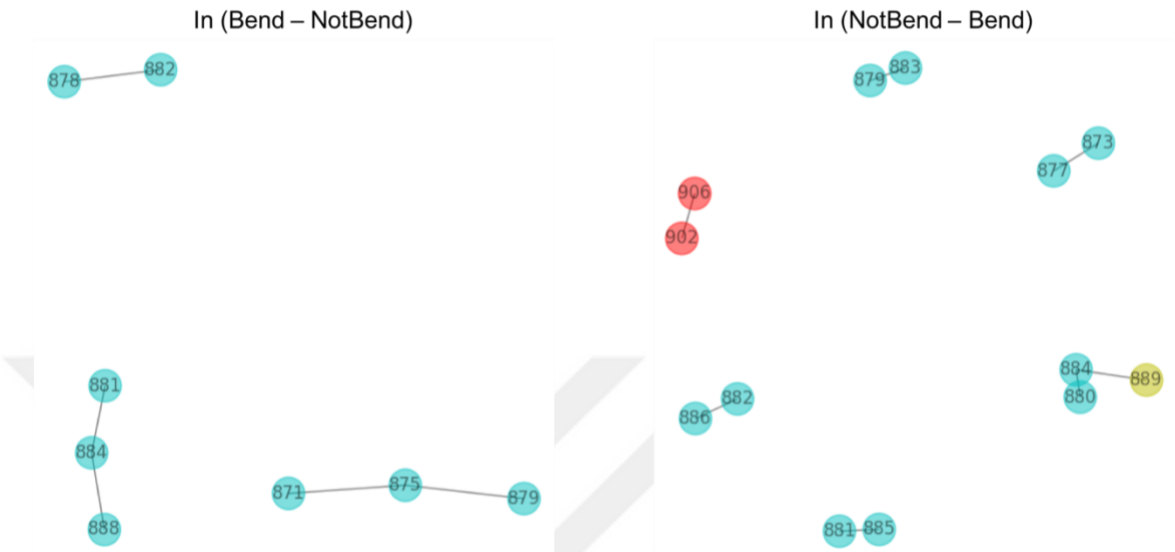

Figure 6.34 : H-bond interactions between H10, H11, the loop, and H12 in CMD simulations. The network on the left shows interactions that are visible in Bend state of H11 and not in NotBend state. The network on the right however, shows interactions that are in NotBend state and not in Bend state. The loop region is shown with yellow nodes. H12 is in red. And cyan colors correlate to residues on H10, and H11.

Also, results of h-bond analysis for AMD simulations suggest that more or stronger interactions between H3 (residues LEU701-ASN705) and H10 (residues 883-888), is due loss of the bend in H11 (Figure 6.35).

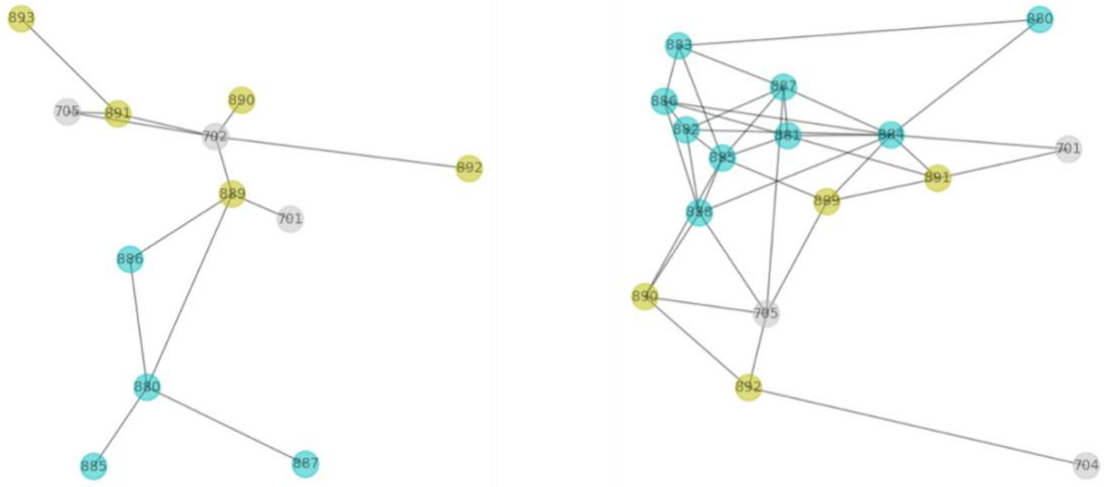

Figure 6.35 : Hbond analysis in AMD simulations separated by Bend and NotBend states. Bend in left, and NotBend in right.

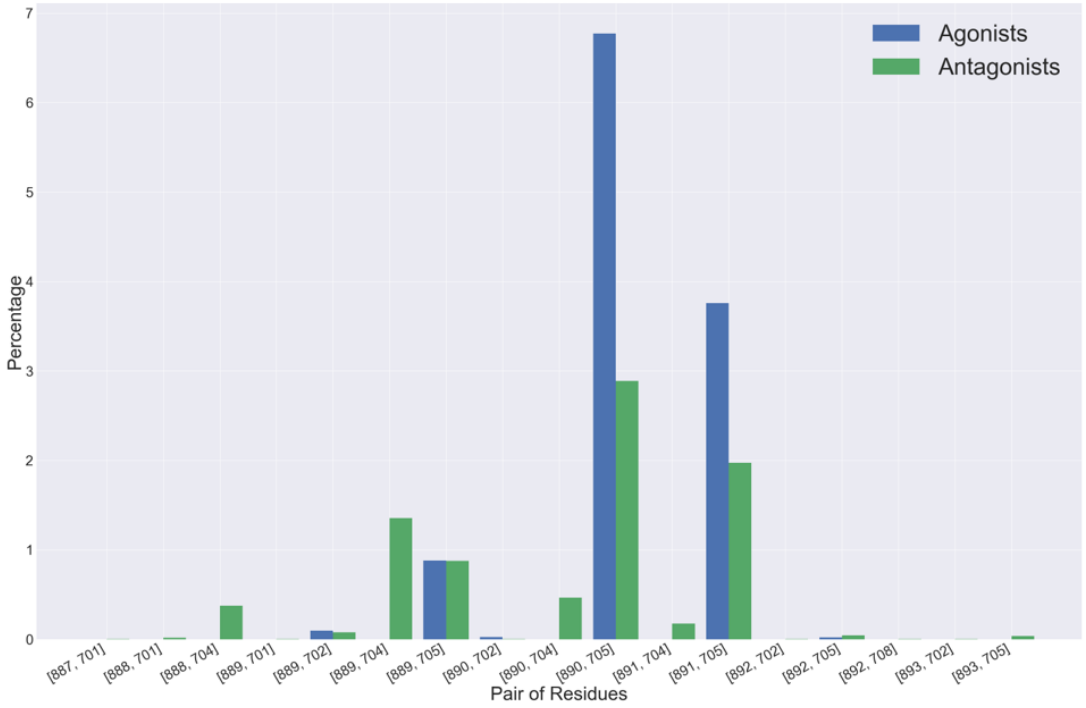

Figure 6.36 : Hbond analysis in AMD simulations separated by agonists and antagonists.

Figure 6.36, also supports the hypothesis that in transition from Bend (agonistic activity) to NotBend (antagonistic activity), interactions between residues 890-891 and ASN705 breaks or weakens. A distribution of interaction scores from Pycontact analysis along all AMD simulations is shown in Figure 6.37. Note that the interaction scores in agonistic state of H11 are higher.

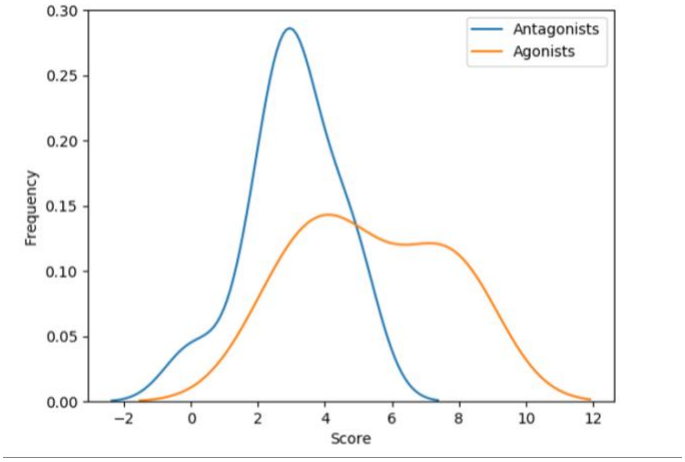

Figure 6.37 : Interactions between residues 891 and N705 in AMD simulations according to Pycontact analysis.

7. FREE ENERGY PERTURBATION (FEP) SIMULATIONS

The purpose of a FEP simulations is to calculate binding energies which in the case of this study, is to calculate binding energies of ligands into AR. FEP simulations are done in two steps of forward and backward FEP simulations. The system includes a protein inside a solution box, and a ligand bound into the protein. In forward FEP simulations the ligand is eliminated from the protein in small timescales. Then a backward FEP simulation by means of adding the ligand into the LBP is done. Then, the difference in free energy of the two systems provides binding energy of the ligand into the protein inside the solution box. Besides, another FEP simulation is considered, where the ligand alone is in a solution box. The results of this simulation is free energy of the ligand inside the solution. The difference in free energies of the ligand bound into the protein and that of the ligand inside the solution is the binding energy of the ligand into the protein.

7.1. FEP Simulations

There were twelve AR-ENZ systems, as follows in Table 7.1. Notice that there are five simulations that were started by docking ENZ into structures of the first five clusters of AR- APO simulations. The last frames of MD simulations (after 1μs) were considered as the starting structures for FEP simulations.

Table 7.1 : AR-ENZ systems for FEP simulations.

Structure	Activity	Structure	Activity
WT	Antagonist	APO1 (3μs-long)	Antagonist
F876I	Agonist	c0-ENZ	Antagonist
F876L	Agonist	c1-ENZ	Antagonist
F876Y	Antagonist	c2-ENZ	Antagonist
T877A	Antagonist	c3-ENZ	Antagonist
T877A/F876L	Agonist	c4-ENZ	Antagonist

A couple of trial simulations were run for an AR-TES system with different timescales and parameters in order to find best parameters for running the simulations (Table 7.2).

Table 7.2 : AR-TES FEP simulation results.

TES System	Description	Lambda	Number of lambda	Simulation step	Equilibration	Total (ns)	Delta G (kcal/mol)
TES_S	TES in solution	0.0625	16	4,250,000	250,000	136	-7.69
TES_S-replica	TES in solution	0.05	20	250,000	50,000	10	-7.50
TES_S-NoCLVR	TES in solution	0.0625	16	4,250,000	250,000	136	-7.67
TES1-1st	First FEP simulation of TES1 MD simulation	0.05	20	250,000	50,000	10	-13.46
TES1-2nd	Second FEP simulation of TES1 MD simulation	0.05	20	500,000	100,000	20	-13.68
TES1-3rd	Third FEP simulation of TES1 MD simulation	0.05	20	750,000	150,000	30	-13.46
TES1-4th	Fourth FEP simulation of TES1 MD simulation	0.05	20	1250,000	250,000	50	-13.44
TES1-10ns	FEP simulation of 10 ns long TES1 MD simulation	0.05	20	250,000	50,000	10	-16.68
TES2	FEP simulation of TES2 MD simulation	0.05	20	250,000	50,000	10	-16.57
TES3	FEP simulation of TES3 MD simulation	0.05	20	250,000	50,000	10	-13.44
TES4	FEP simulation of TES4 MD simulation	0.05	20	250,000	50,000	10	-15.58

In Table 7.3, the first three systems are TES in solution, that in one of them, the constraint in order to keep the ligand in the center of the solution box was not applied (TES_S-NoCLVR). Meanwhile, as it is shown in the Delta G column, no significant difference is visible in its binding energy. Another noteworthy point is that longer FEP simulations does not necessarily provide better results.

Exceptionally, in one system (TES1-10ns) the starting structure of the system was taken after 10ns of a MD simulation. Starting a FEP simulation after a short MD simulations provides different binding energy due to different structure. As a conclusion a 10ns simulation seemed to be long enough to find binding energies of ligands in the protein. Moreover, 0.05 as the lambda value, 20 as the number of lambda, 50,000 equilibration

steps, and 250,000 simulation steps were considered for further simulations. For the validation of FEP simulation results, one must compare them to experimental results. In the case of TES-binding affinity, the experimental result is about -5.26 kcal·mol–1. This binding affinity was calculated using the K_d value. [19]. This binding affinity validates our calculated binding energy of TES into AR-LBP in our simulation, which is around -5.77 kcal·mol–1 according to calculations below.

$$\Delta G_{TES\ bound\ into\ protein\ inside\ solution} = -13.46$$

$$\Delta G_{TES\ in\ solution} = -7.69$$

$$\Delta G_{Binding\ Energy\ of\ TES} = \Delta G_{TES\ bound\ into\ protein\ inside\ solution} - \Delta G_{TES\ in\ solution} \quad (7.1)$$

In total, we considered 36 simulations that were run for 12 AR-ENZ systems. (Table 7.1). Clustering analysis were run for three replicas of each system, and the first five clusters of them (in total, 60 structures) were chosen for further FEP simulations. Appendix 1, is depictions of CMD FEP simulation results together with their binding pose. Note that among systems with names starting with c0-ENZ, the first system (c0-c0) is the most dominant system, thus it is important due to the fact that it is the most promising candidate for a WT structure of AR.

7.2. Analysis of FEP Results

Table 7.3 shows the FEP results of CMD and AMD simulations altogether. Note that in this section, only the first structure of 5APOs is included. According to Figure 7.1, ENZ has higher binding energy upon binding into antagonist AR than agonist AR. This also validate the fact that ENZ as an antiandrogen binds better to an antagonist AR.

Table 7.3 : Binding energies obtained from FEP simulations of AR-ENZ simulations (kcal/mol).

System	AMD	CMD	System	AMD	CMD	System	AMD	CMD
APO1-c0	-20.28	-19.23	F876I-c0	-21.57	-20.87	T877-F876L-c0	-26.95	-27.35
APO1-c1	-24.81	-23.87	F876I-c1	-24.50	-17.05	T877-F876L-c1	-28.50	-28.12
APO1-c2	-21.93	-21.42	F876I-c2	-24.39	-19.63	T877-F876L-c2	-28.13	-27.44
APO1-c3	-22.42	-18.69	F876I-c3	-24.42	-22.17	T877-F876L-c3	-27.56	-10.72
APO1-c4	-23.24	-23.20	F876I-c4	-22.39	-19.20	T877-F876L-c4	-27.51	-26.64
c0-ENZ-c0	-28.92	-20.40	F876L-c0	-22.92	-21.6	T877A-c0	-30.89	-27.35
c0-ENZ-c1	-22.74	-26.23	F876L-c1	-27.31	-21.58	T877A-c1	-30.54	-23.36
c0-ENZ-c2	-23.94	-20.64	F876L-c2	-22.46	-19.55	T877A-c2	-28.94	-25.59
c0-ENZ-c3	-20.52	-21.16	F876L-c3	-24.92	-28.51	T877A-c3	-26.92	-27.79
c0-ENZ-c4	-20.63	-24.70	F876L-c4	-23.41	-27.60	T877A-c4	-30.73	-24.89
			F876Y-c0	-28.72	-28.39	WT-c0	-26.72	-30.17
			F876Y-c1	-27.93	-28.92	WT-c1	-31.50	-29.61
			F876Y-c2	-26.64	-28.13	WT-c2	-31.85	-26.50
			F876Y-c3	-27.84	-26.23	WT-c3	-27.41	-28.66
			F876Y-c4	-29.08	-26.60	WT-c4	-29.98	-24.89

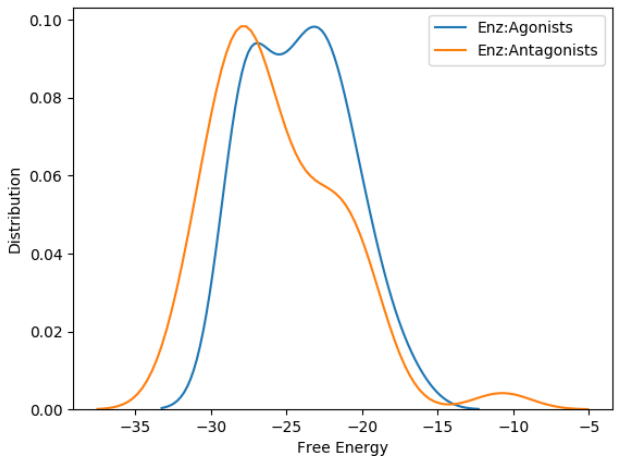

Figure 7.1 : Distribution of binding Energies extracted from FEP simulation results.

8. DISCUSSION

Results of CMD and AMD simulations suggest that, upon antagonist binding, pathway of interactions that lead to movement on H12, differ from those in agonist binding. When ENZ binds into an antagonist AR-LBP, interactions between enzalutamide and residues L701 (hydrophobic or h-bond), and N705 (h-bond) result in breaking down the interactions between residues L701, N705, and residue F891(h-bond) on the loop between H11 and H12. This leads to more distance between H3, and the loop between H11 and H12. Furthermore, due to more flexibility of the loop, H12 moves away from H3, thus moving outwards LBP. Movement of H12 distorts the AF2 site of AR, thus making it an improper site for the coactivator to bind (Figure 8.1). Moreover, the normal transcriptional activity of AR is suppressed. FEP simulation results also showed that ENZ binds stronger into AR-antagonists than AR-agonists.

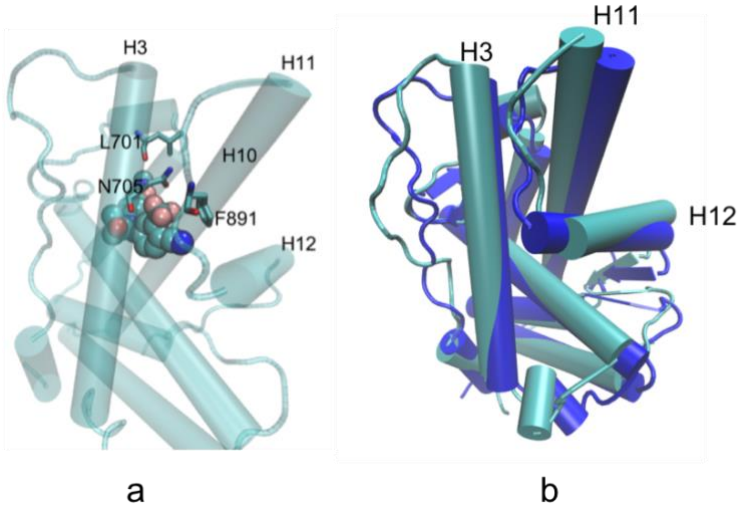

Figure 8.1 : a) Pathway of interactions upon ENZ binding. b) Movement of H12. Bend in blue, and NotBend in cyan.

9. CONCLUSION

Enzalutamide molecule is the most recent and potent drug in treatment of prostate cancer. However, despite its success in treatment of prostate cancer, drug resistance occurs due to two point mutations, F876I, and F876L, that abolish the antagonistic activity of enzalutamide. The molecular mechanisms of this resistance remain elusive. Thus, this study investigated the mechanism of this resistance at the molecular level using molecular dynamics simulations. We performed dockings of ENZ into WT-AR, and several AR mutants structures. Furthermore, we performed one micro-second long classical and accelerated MD simulations considering replicas for every system. Our simulations suggest that unbending of H11 (in the crystal structure, it is in bend state) leads to loss in stability of H12. In the simulations of Apo AR and AR with Testosterone, the unbending is rare. On the contrary, the simulations of AR with enzalutamide, particularly with mutations abolishing antagonist activity, the unbending of H11 becomes too frequent. The current study found a pathway of interactions that lead to drug resistance upon enzalutamide binding. These findings is believed to be important for future studies in the subject, and for new drug developments for treatment of prostate cancer.

REFERENCES

[1] **Ark, A. V., Cao, J., and Li, X.,** 2018: Mechanisms and Approaches for Overcoming Enzalutamide Resistance in Prostate Cancer. *Frontiers in Oncology* 8, 1 – 8.

[2] **Korpal1, M., Korn1, J. M., Gao, X., Rakiec, D. P., Ruddy, D. A., Doshi, S., Yuan, J. , Kovats, S. G., Kim, S., Cooke, V. G., Monahan, J. E., Stegmeier, F., Roberts, T. M., Sellers, W. R., Zhou, W., and Zhu, P.,** 2013: An F876L Mutation in Androgen Receptor Confers Genetic and Phenotypic Resistance to MDV3100 (Enzalutamide). *American Association for Cancer* 3(9), 1 – 33.

[3] **Balbas, M. D., Evans, M. J., Hosfield, D. J., Wongvipat, J., Arora, V. K., Watson, P. A., Chen, Y., Greene, G. L., Shen, Y., and Sawyers, C. L.,** 2013: Overcoming mutation-based resistance to antiandrogens with rational drug design. *eLife* 2, 1 – 21.

[4] **Ferlay, J., Shin, H.R., Bray, F., Forman, D., Mathers, C., and Parkin, D.M.,** 2010: Estimates of worldwide burden of cancer in 2008: GLOBOCAN 2008. *Int. J. Cancer* 127, 2893 – 2917.

[5] **Bassetto, M., Ferla, S., Pertusati, F., Kandil, S., Westwell, A. D., Brancale, and A., McGuigan, C.,** 2016: Design and synthesis of novel bicalutamide and enzalutamide derivatives as antiproliferative agents for the treatment of prostate cancer. *European Journal of Medicinal Chemistry* 118, 230 – 243.

[6] **Liu, N., Zhou, W., Guo, Y., Wang, J., Fu, W., Sun, H., Li, D., Duan, M., and Hou**, **T.,** 2018: Molecular Dynamics Simulations Revealed the Regulation of Ligands to the Interactions between Androgen Receptor and Its Coactivator, *Journal of Chemical Information and Modeling* 58, 1652 – 1661.

[7] **Duan, M., Liu, N., Zhou, W., Li, D., Yang, M., and Hou**, **T.,** 2016: Structural Diversity of Ligand-Binding Androgen Receptors Revealed by Microsecond Long Molecular Dynamics Simulations and Enhanced Sampling. *J. Chemical Teory and Computation* 12, 4611 – 4619.

[8] **Prekovic, S., Royen, M. E., Voet, A. R., Geverts, B., Houtman, R., Melchers, D., Zhang, K. Y.J., Broeck, T. V., Smeets, E., Spans, L., Houtsmuller, A. B., Joniau, S., Claessens, F., and Helsen**, **Ch.,** 2016: The Effect of F877L and T878A Mutations on Androgen Receptor Response to Enzalutamide. *Mol Cancer Ther* 15, 1702 – 1712.

[9] **Paul, N., Carabet, L. A., Lallous, N., Yamazaki, T., Gleave, M. E., Rennie, P. S., and Cherkasov**, **A.,** 2016: Cheminformatics Modeling of Adverse Drug Responses by Clinically Relevant Mutants of Human Androgen Receptor. *J. Chem. Inf. Model* 56, 2507 − 2516.

[10] **Liu, H., Wang, L., Tian, J., Li, J., and Liu**, **H.,** 2017: Molecular Dynamics Studies on the Enzalutamide Resistance Mechanisms Induced by Androgen Receptor Mutations. *Journal of Cellular Biochemistry* 118, 2792 – 2801.

[11] **Sakkiah, S., Kusko, R., Pan, B., Guo, W., Ge, W., Tong, W, and Hong, H.,** 2018: Structural Changes Due to Antagonist Binding in Ligand Binding Pocket of Androgen Receptor Elucidated Through Molecular Dynamics Simulations. *Frontiers in Pharmacology* 9, 492.

[12] **Jo, S., Kim, T., Iyer, V.G., and Im, W.,** 2008: CHARMM-GUI: A Web-based Graphical User Interface for CHARMM. *J. Comput. Chem*. 29, 1859 – 1865.

[13] **Phillips, J. C., Braun, R., Wang, W., Gumbart, J., Tajkhorshid, E., Villa, E., Chipot, Ch., Skeel, R. D., Kale, L., and Schulten, K.,** 2005: Scalable molecular dynamics with NAMD. *Journal of Computational Chemistry* 26, 1781 – 1802.

[14] **Morris, G. M., Huey, R., Lindstrom, W., Sanner, M. F., Belew, R. K., Goodsell, D. S., and Olson, A. J.,** 2009: Autodock4 and AutoDockTools4: automated docking with selective receptor flexibility. *J. Computational Chemistry* 16, 2785 – 2791.

[15] **Case, D.A., Cheatham, T.E., Darden, T., Gohlke, H., Luo, R., Merz, K.M., Jr., Onufriev, A., Simmerling, C., Wang B., and Woods, R.,** 2005: The Amber biomolecular simulation programs. *J. Computat. Chem.* 26, 1668 – 1688.

[16] **Scheurer, M., Rodenkirch, P., Siggel, M., Bernardi, R. C., Schulten, K., Tajkhorshid, E., and Rudack, T.,** 2018: PyContact: Rapid, Customizable, and Visual Analysis of Noncovalent Interactions in MD Simulations. *Biophysical Journal* 114(3), 577-583.

[17] **Humphrey, W., Dalke, A., and Schulten, K.,** 1996: VMD - Visual Molecular Dynamics, *J. Molec. Graphics* 14, 33-38.

[18] **F. Fratev,** 2015: Activation helix (H12) orientation of the estrogenreceptor is mediated by receptor dimerization: evidence from molecular dynamics simulations. *J. Physical Chemistry Chemical Physics*, 17(20), 13403 – 13420.

[19] **Muddana, S. S., Price, A. M., MacBride, M. M., and Peterson, B. R.,** 2004: 11beta-alkyl-Delta9-19-nortestosterone derivatives: high-affinity ligands and potent partial agonists of the androgen receptor. *J. Med Chem*, 47(21) 4985 – 4988.

APPENDICES

APPENDIX A.1 : Binding Energies

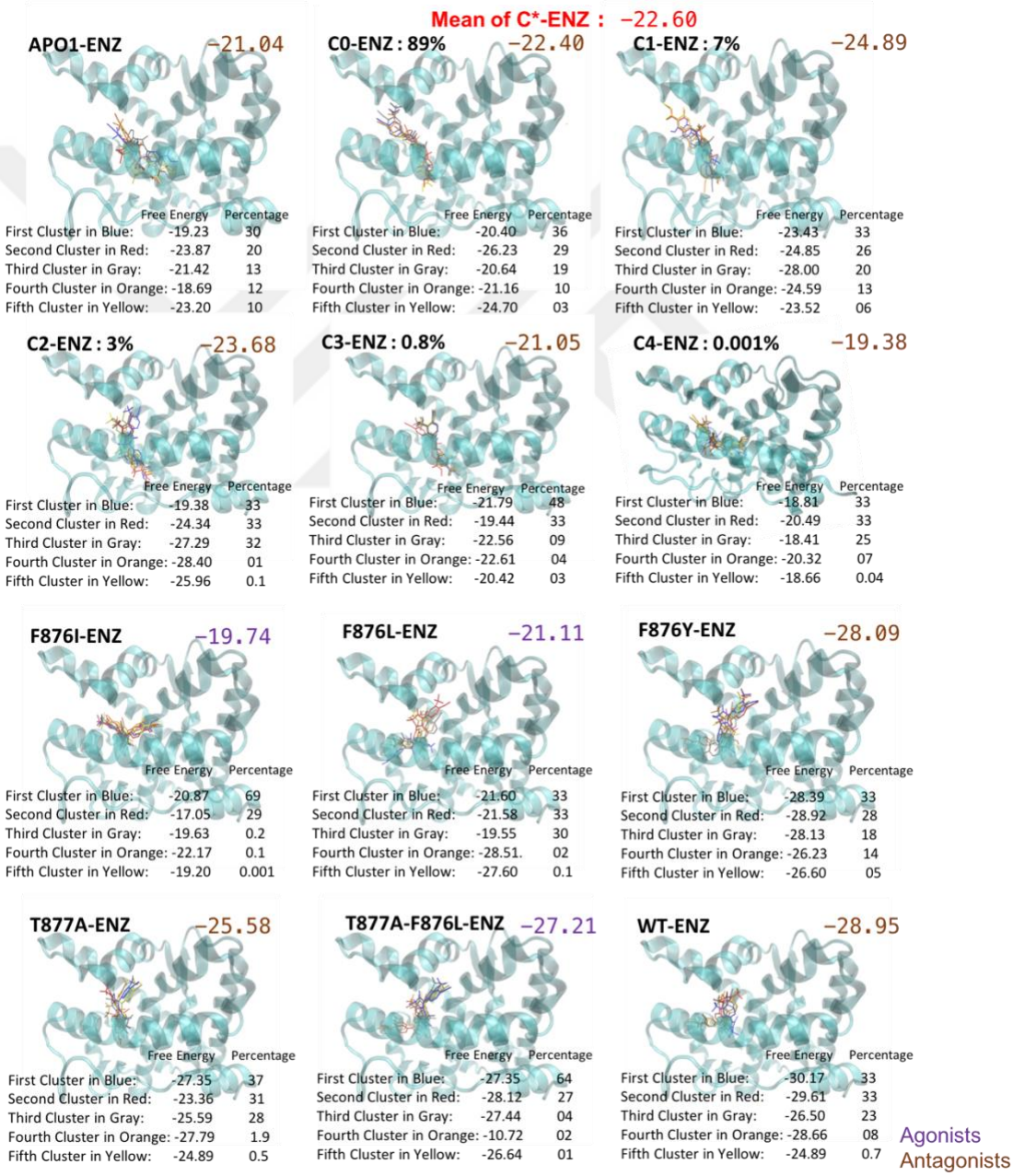

Figure A.1 : Binding energies together with binding poses of ENZ within AR-LBP in CMD simulations.

CURRICULUM VITAE

Name Surname: Behzad Aslani Avilaq

Place and Date of Birth: Tabriz, Iran

Address: Istanbul Technical University, Istanbul, Turkey

E-Mail: Avilaq16@itu.edu.tr

B.Sc.: Applied Informatics

Professional Experience and Rewards: working on a research project funded by TUBITAK; 2017-2020